



Published in final edited form as:

Nat Genet. 2020 February ; 52(2): 146–159. doi:10.1038/s41588-019-0575-8.

Slipped-CAG DNA binding small molecule induces trinucleotide repeat contractions *in vivo*

Masayuki Nakamori^{1,12}, Gagan B. Panigrahi^{2,12}, Stella Lanni^{2,12}, Terence Gall-Duncan^{2,3}, Hideki Hayakawa¹, Hana Tanaka¹, Jennifer Luo^{2,3}, Takahiro Otabe⁴, Jinxing Li⁴, Akihiro Sakata⁴, Marie-Christine Caron^{5,6}, Niraj Joshi^{5,6}, Tanya Prasolava², Karen Chiang^{2,3}, Jean-Yves Masson^{5,6}, Marc S. Wold⁷, Xiaoxiao Wang⁸, Marietta Y. W. T. Lee⁸, John Huddleston^{9,10}, Katherine M. Munson⁹, Scott Davidson², Mehdi Layeghifard², Lisa-Monique Edward², Richard Gallon¹¹, Mauro Santibanez-Koref¹¹, Asako Murata⁴, Masanori P. Takahashi¹, Evan E. Eichler^{9,10}, Adam Shlien², Kazuhiko Nakatani⁴, Hideki Mochizuki¹, Christopher E. Pearson^{2,3,*}

¹Department of Neurology, Osaka University Graduate School of Medicine, Osaka, Japan.

²Program of Genetics & Genome Biology, The Hospital for Sick Children, The Peter Gilgan Centre for Research and Learning, Toronto, ON, Canada.

³University of Toronto, Program of Molecular Genetics, Toronto, ON, Canada.

⁴Department of Regulatory Bioorganic Chemistry, The Institute of Scientific and Industrial Research, Osaka University, Osaka, Japan.

⁵Genome Stability Laboratory, CHU de Québec Research Center, HDQ Pavilion, Oncology Division, Québec City, QC, Canada.

⁶Department of Molecular Biology, Medical Biochemistry and Pathology, Laval University Cancer Research Center, Québec, QC, Canada.

⁷Department of Biochemistry, Carver College of Medicine, University of Iowa, Iowa City, IA, USA.

⁸Department of Biochemistry and Molecular Biology, New York Medical College, Valhalla, NY, USA.

⁹Department of Genome Sciences, University of Washington, Seattle, WA, USA,

Users may view, print, copy, and download text and data-mine the content in such documents, for the purposes of academic research, subject always to the full Conditions of use:http://www.nature.com/authors/editorial_policies/license.html#terms

* cepearson.sickkids@gmail.com.

AUTHOR CONTRIBUTIONS

M.N. performed repeat length analysis, cell and mouse treatments. G.B.P. performed replication, repair, footprinting and R-loop processing. S.L. performed NA binding, repeat instability analysis, protein-interactions, polymerase δ extension assay, and instability index assessment. H.H., H.T., M.P.T., and H.M. performed mouse treatments. T.O., J. Li, A.S., A.M., and K.N. synthesized, purified and characterized NA. J. Luo and T.P. performed cell treatments. T.G.-D. performed assessment of NA on mHTT aggregates, HTT translation, and TUNEL assay. M.-C.C., N.J., J.-Y.M., M.S.W., X.W., and M.Y.W.T.L. performed protein purification. S.L., G.B.P., and K.C. performed *in vitro* repair/binding assays. J.H., K.M.M., and E.E.E. performed single-molecule sequencing and bioinformatic analysis. R.G. and M.S.-K. performed microsatellite instability assay. S.D., M.L., L.-M.E., and A.S. performed whole genome sequencing and mutation signature analysis. C.E.P., M.N., K.N., G.B.P., and S.L. conceived experiments, analyzed data and wrote the manuscript. M.N., G.B.P. and S.L. contributed equally to the study. All authors discussed the results and commented on the manuscript.

COMPETING INTERESTS STATEMENT

The authors declare no competing financial interests.

¹⁰Howard Hughes Medical Institute, University of Washington, Seattle, WA, USA.

¹¹Institute of Genetic Medicine, Newcastle University, Newcastle upon Tyne, UK

¹²These authors contributed equally to this work.

Abstract

In many repeat diseases, like Huntington's disease (HD), ongoing repeat expansions in affected tissues contribute to disease onset, progression and severity. Inducing contractions of expanded repeats by exogenous agents is not yet possible. Traditional approaches would target proteins driving repeat mutations. Here we report a compound Naphthyridine-Azaquinolone (NA) that specifically binds slipped-CAG DNA intermediates of expansion mutations, a previously unsuspected target. NA efficiently induces repeat contractions in HD patient cells as well as *en masse* contractions in medium spiny neurons of HD mouse striatum. Contractions are specific for the expanded allele, independent of DNA replication, require transcription across the coding CTG strand, and arise by blocking repair of CAG slip-outs. NA-induced contractions depend upon active expansions driven by MutS β . NA injections in HD mouse striatum reduce mutant HTT protein aggregates, a biomarker of HD pathogenesis and severity. Repeat structure-specific DNA ligands are a novel avenue to contract expanded repeats.

Expansion of unstable trinucleotide repeats causes over 40 neurodegenerative diseases, including Huntington's disease (HD), and 17 of these are caused by gene-specific CAG/CTG trinucleotide repeat expansions^{1–5}. Ongoing repeat expansions in affected tissues correlate with disease age-of-onset, progression and severity^{6,7}, and dramatic repeat length variations exist between tissues of the same individual¹. For at least six CAG diseases (HD, spinocerebellar ataxia type 1 (SCA1), SCA2, SCA3, SCA7, and SCA17), DNA repair proteins are major modifiers of age-of-onset^{8,9} and disease progression¹⁰, suggesting that ongoing somatic expansions contribute to age-of-onset and progression². Therefore, arresting or reversing somatic CAG/CTG repeat expansions may arrest or reverse disease progression². Inheritance of larger HD CAG expansions also leads to earlier age-of-onset and accelerated disease progression^{11,12}. Thus, inducing contractions of the expanded repeat to lengths shorter than the inherited tract length should have beneficial effects.

While the exact mechanism(s) of repeat expansions are unclear, all models involve the aberrant repair of unusual slipped-DNA structures formed by the repeats^{4,13–22}. Slipped-DNAs form by out-of-register annealing of complementary repeat strands during DNA repair, replication or transcription, and have slip-outs with intra-strand hairpins of CAG or CTG repeats^{16,21}. Slipped-DNAs were detected at the mutant myotonic dystrophy (DM1) locus in patient tissues, including the CNS, and were not present at the non-expanded allele¹³. Levels of slipped-DNAs were greatest in tissues showing the largest expansions, supporting the involvement of slipped-DNAs in the expansion processes.

A compound with specificity for slipped-DNAs may alter their formation and/or processing—attributes that could modulate repeat instability. We previously designed a CAG-specific DNA binding compound, Naphthyridine-Azaquinolone (NA)^{23–25}, which binds to a distorted intra-strand CAG hairpin, with the naphthyridine and azaquinolone moieties

forming hydrogen bonds to guanine and adenine, respectively, causing two cytosines to flip-out from the CAG hairpin (Fig. 1a,b)²⁵. NA bound with high affinity and increased the melting temperature of (CAG)10 hairpins by $>30^{\circ}\text{C}$ ²⁴, and preferentially bound to longer (>30) CAG hairpins²⁵. The high selectivity of NA for longer CAG hairpins coupled with the presence of slipped-DNAs at a mutant repeat locus¹³ suggested it may specifically target the expanded allele.

RESULTS

NA binds long CAG slip-out structures.

To determine if NA can bind disease-relevant (CAG)•(CTG) duplexes with and without slip-outs, we performed band-shifts using slipped-DNAs¹⁶ that mimic those at the mutant DM1 locus in patient tissues¹³. NA did not bind to fully duplexed DNAs containing (CAG)50•(CTG)50 repeats, and high concentrations of NA did not induce structural alterations of the DNA (Fig. 1c,d). NA bound molecules of (CAG)50•(CTG)50 with clustered short slip-outs²² to a limited degree, but their short slip-outs and electrophoretic heterogeneity prohibited detection of a single-shifted species (Fig. 1c,d). Slipped-heteroduplexes with a single long slip-out of 20 CAG excess repeats in (CAG)50•(CTG)30 were extensively bound by NA (Fig. 1c,d). NA-binding caused electrophoretic band-broadening, previously observed for other DNA-binding ligands²⁶. The progressively slower migration of the slipped-DNA with added NA is consistent with NA binding to additional (CAG)•(CAG) pairs in the hairpin²⁵. In contrast, DNAs with long slip-outs of CTG repeats, (CAG)30•(CTG)50, were not bound by NA (Fig. 1c,d). Thus, NA specifically bound CAG but not CTG slip-outs. We confirmed this with footprinting experiments using the single-strand DNA-specific mung bean nuclease (MBN), which cleaves only the slip-out regions between the AG of every CAG unit¹⁶ (Fig. 1e). Upon NA binding to the CAG slip-out, MBN digestion is inhibited, with the exception of the hairpin tip (Fig. 1e), not bound by NA. Denaturation of purified slipped (CAG)50•(CTG)30 to individual (CAG)50 and (CTG)30 single-strands showed NA binding specifically to the single-stranded (CAG)50 strand (Fig. 1f). Subsequent renaturation of the individual single-strands revealed that NA did not block complementary strand hybridization, but bound specifically to the slipped-out CAG strand (Fig. 1f). The greater degree of electrophoretic shift of the isolated single-stranded (CAG)50 tract compared to (CAG)50•(CTG)30 is caused by it being forced into a long hairpin of 50 repeats that can bind more NA molecules. Note that the amount of NA bound to (CAG)50•(CTG)30 or (CAG)50 following re-hybridization (Fig. 1f, 7.5 μM NA) is considerably greater than in the absence of re-hybridization (Fig. 1c, 50 μM NA), even though the amount of NA is more than 5-fold higher in the latter. These results suggest that, in biological situations where the CAG repeat is denatured from its complementary CTG strand, the full-length of the isolated CAG tract would become fully bound by NA in a hairpin-like conformation. Furthermore, NA binding was significantly greater for longer CAG slip-outs (Supplementary Fig. 1). We previously estimated a ratio of two NA molecules to one CAG-CAG, wherein a slip-out of (CAG)20 would bind maximally 20 NA molecules²⁵. The molar ratio of 2:1 NA to slipped-out repeats was evident for the longer slip-outs. Affinity of each NA molecule/CAG-CAG was estimated as $1.8 \times 10^6 \text{ M}^{-1}$ as K_a or $0.56 \times 10^{-6} \text{ M}$ as K_d ²⁵. NA can be removed from the DNA using phenol/chloroform

extraction (Extended Data Figure 4c). Together, these findings support the structure-specificity of NA for long CAG repeat slip-outs of disease-relevant tract lengths, and indicate that NA does not induce slip-out extrusion from an expanded fully duplexed molecule, but induces formation of longer slip-outs from a single-stranded CAG tract.

NA inhibits repair of long CAG slip-outs.

We tested whether NA could block processing of slipped-DNAs, which could forecast its ability to modify repeat instability. NA specifically inhibited repair of slipped-DNAs with long (CAG)20 slip-outs, but not (CTG)20 slip-outs (Fig. 2a–c). This specificity is consistent with the inability of DNA polymerases to extend primers along NA-bound (CAG)20 templates^{23,24}. We assessed the effects of NA on repair of a single extra CAG repeat slip-out, too small to be bound by NA. Repair of this substrate was unaffected by NA (Fig. 2d and Supplementary Fig. 1), consistent with its binding specificity for long slip-outs. NA did not bind to slip-outs of 3 excess repeats, but binding could be detected for 5, 11, 15, or 20 excess CAG repeats, with increased binding for slip-outs >10 (Supplementary Fig. 1, upper panel). Repair of DNA substrates with a similar range of slip-out sizes from 6, 10, 13, or 20 excess CAG repeats was inhibited by NA (Supplementary Fig. 1, lower panel), indicating that, once the DNA is bound by NA, repair is inhibited and not further altered by increased NA-bound lengths. These data suggest that there is a less-than-additive effect for both NA binding and NA's effect on slip-out repair. NA had no effect on repair of a G-T mismatch, the most frequent base-base mismatch, which depends upon mismatch repair (MMR) proteins^{22,27} (Fig. 2e). Thus, NA is unlikely to cause genome-wide mutations that occur in the absence of MMR.

NA modulates instability of expanded mutant repeats in HD cells, with limited off-target effects.

At 50 μ M, NA is cell-permeable and enters nuclei without causing acute or long-term cytotoxicity, slowing proliferation, or altering DNA replication or transcription across CTG tracts (Fig. 3a–c and Extended Data Fig. 1). Tract lengths of >200 repeats are frequent in brain cells that have experienced somatic expansions in HD individuals that inherited (CAG)40–50^{1,7,28}. NA induced a significant shift in repeat population towards contraction of a (CAG)180•(CTG)180 tract at the *HTT* locus in HD patient-derived primary fibroblasts⁵. NA enhanced the number of contractions of the expanded HD repeat (Fig. 3d; $P = 7.25 \times 10^{-6}$, Supplementary Table 1), causing significant repeat loss (Fig. 3f; $P = 0.0003$). NA also induced a significant reduction in the number of expansions of the HD repeat (Fig. 3d; $P = 4.34 \times 10^{-5}$, Supplementary Table 1). We also treated HD patient fibroblasts with (CAG)43, a mutation length common in the majority of patients. A significant number of NA-treated cells showed contractions of the expanded repeat, with contractions as low as 20 repeats, below the HD disease threshold of 35 units (Fig. 3e,g; $P = 3.28 \times 10^{-5}$, Supplementary Table 1). NA also reduced the number of expansions (Fig. 3e; $P = 8.32 \times 10^{-5}$, Supplementary Table 1). Thus, NA can induce contractions of expanded tract lengths common in inherited and somatically expanded HD alleles. In contrast, NA does not affect either the non-expanded HD repeat or other microsatellite repeats known to be prone to instability under stressed conditions (Fig. 3h and Extended Data Fig. 2a), suggesting that NA is specific for

structures formed by expanded CAG/CTG repeats and will not deleteriously affect other repeats.

As an additional control, we first assessed the effect of NA at the very long but genetically stable (i.e., not forming slipped-DNA structures) CAG tract of the *TBP* gene in HD patient cells. Stretches of >49 CAG repeats at the *TBP* locus cause fully-penetrant SCA17 disease²⁹. Our HD cell lines have 43 unstable repeats at the *HTT* gene and a similar length of 38 and 34 stable repeats of the non-mutant *TBP* gene. NA did not change the length distribution of *TBP* repeats^{30,31} (Extended Data Fig. 2d and Supplementary Table 1), further supporting its specificity for actively unstable tracts that form slipped-DNAs.

To assess possible mutagenic activity of NA, we assessed its effect on a cancer diagnostic MSI panel of >20 slippage-prone mononucleotide repeats, using a sequencing-based assay capable of detecting low-level microsatellite instability in non-neoplastic tissues³². There was no evidence of increased MSI from NA treatment in either HD cells with (CAG)43 or (CAG)180 (Extended Data Fig. 2f). As a control for non-repetitive regions, we assessed the *HPRT1* gene (exons 2 to 3), which is an established surrogate for evaluating mutagen-induced mutation spectra^{33–36}. Since *HPRT1* is on the X-chromosome, each of multiple single long-read sequences of *HPRT1* can be used as a proxy for a single cell in male HD cells (GM09197, (CAG)180/21), permitting assessment of the effect of NA on individual cells without overlapping alleles. We sequenced up to 2,402 individual *HPRT1* alleles in three independent replicates and found no sequence differences between NA- and mock-treated cells (Extended Data Fig. 3a–c). We also assessed whether NA could induce an unsuspected mutation signature in HD cells ((CAG)43 or (CAG)180) using whole-genome sequencing. Environmental and anti-cancer agents can lead to specific mutation signatures^{37–39}. We screened the NA-treated and untreated HD cells for mutational signatures shown in COSMIC using an established pipeline (SigProfiler version 0.0.5.75⁴⁰). We were unable to detect a statistically significant mutation signature. The genome of NA-treated HD cells showed very low numbers of single or double substitutions (SBS or DBS) or insertions/deletions (INDELs), and no rearrangements (Fig. 3i). The SBS/INDELs/DBS/rearrangements for the (CAG)43 and (CAG)180 cells were 172/29/7/0 and 187/42/5/0, respectively. Similar background mutations attributed to DNA damage incurred during cell culture (~245 SBS, ~35 INDELs, ~6 DBS, and ~0 rearrangements per genome) have been detected^{41–43}. Moreover, cells treated for 24 hours with the food additive potassium bromate (875 μ M) or the anticancer drug cisplatin (12.5 μ M) showed ~576/~31 and ~926/~65 SBS/INDELs, respectively⁴¹, both substantially “noisier” than our experiment treating HD cells with NA chronically for 40 days (50 μ M). The “silence” of NA off-target mutagenesis is contrasted by the “noisy” mutational burden of the hyper- and ultra-hyper-mutated genomes of brain cancers of MMR-deficient individuals assessed by the same pipeline^{44–48}—a portent of non-specific targeting of MutS β (Fig. 3i). Together, these results argue against NA as a general mutagen.

Effect of NA depends on transcription but not replication through the repeat tract.

NA could affect repeat instability during replication or transcription. NA treatment induced a significant shift in repeat population towards contraction of a (CAG)850•(CTG)850 tract in

human cells, expressing r(CAG)850²⁰ (Fig. 4a,b; $P = 4.78 \times 10^{-5}$, Supplementary Table 1), and significantly shortened the average size of the repeat tract, with losses of up to 790 repeats (Fig. 4b; $P = 6.44 \times 10^{-3}$). NA's effects were independent of cell proliferation and DNA replication, as near-complete arrest of proliferation using Palbociclib, contact inhibition, or serum starvation had no effect on NA-induced CAG contractions (Fig. 4d,e and not shown). This is consistent with NA's lack of effect on cell proliferation (Fig. 3c) or replication fork progression (Extended Data Fig. 1). To address the requirement for transcription, we used an established cell model, HT1080-nontranscribing (CAG)850, having a single (CAG)850 transgene floxed by transcription-terminator elements, so that the expanded repeat is not transcribed in either direction^{20,49}. We confirmed the absence of transcription (Fig. 4c) and treated cells with NA in transcribing or non-transcribing conditions. NA only induced contractions of the (CAG)850 tract when transcription was permissible (Fig. 4b,f). Since NA did not alter transcription across the expanded repeat, either in these cells or HD patient fibroblasts (Fig. 4g and Extended Data Fig. 4a), this shows that NA induces CAG contractions during transcription across the expanded repeat, consistent with transcription having a driving role in inducing CAG instability and NA-induced contractions^{15,20,50,51}. The ability of NA to induce contractions required transcription across the CTG repeat, but did not involve arrest of transcription. Again, NA did not affect non-expanded CAG/CTG tracts or other microsatellite repeats in the HT1080 cell model (Extended Data Fig. 2b,c). Thus, NA depends upon transcription across the expanded repeat to induce repeat contractions, and is effective independent of cell proliferation.

NA does not block *in vitro* R-loop formation, R-loop stability, or RNase digestion, but enhances formation of repeat contractions.

Transcription-induced R-loops can lead to CAG/CTG instability^{17,20} and may cause the transcription dependency of NA on repeat instability. NA did not alter transcript levels of the expanded repeat or translation of the mutant Huntingtin protein in cells (Extended Data Fig. 4a,b), nor did it affect transcription *in vitro* (Supplementary Fig. 2a–d). NA (120 μ M) did not affect R-loop formation, nor RNaseA or RNaseH processing of pre-formed R-loops (Supplementary Fig. 2c,d). At NA concentrations used on cells (50 μ M), R-loops remained detectable, suggesting NA does not affect R-loop biophysical stability (Supplementary Fig. 2d). However, NA altered processing of CAG/CTG R-loops in extracts of neuron-like human SH-SY5Y cells, significantly increasing the number of contraction products with a milder effect on expansion products (Extended Data Fig. 5a–c, $P = 0.002$ vs. $P = 0.04$). These results suggest NA causes preferential R-loop processing to repeat contractions.

NA alters activity of several DNA repair proteins on long CAG slip-outs.

NA could block interaction of DNA repair proteins with slipped-DNAs, similar to its ability to block MBN activity on (CAG)20 slip-outs (Fig. 1e). As the proteins involved in large (CAG)20 slip-out repair are unknown, we assessed four candidate proteins MutS β , RPA, pol δ and pol β . In mice, the mismatch repair MutS β complex (MSH2-MSH3) with a functioning ATPase drives CAG/CTG expansions^{2,3,19,52,53}. MSH3 is a modifier of age-of-onset and disease progression in HD patients, and a modifier of repeat instability in HD and DM1 patients^{54,55}. MutS β is not required to repair long (CAG)10–25 slip-outs^{22,27,56,57}, but

may be involved in formation of slipped-DNAs following resolution of transcriptionally induced R-loops^{21,56,58}. This process, expected to involve MutS β binding to DNA and ATP-mediated dissociation of the MutS β -DNA complex, may be affected by NA. NA did not block binding of MutS β to long CAG slip-outs, nor did NA affect the ATP-mediated dissociation of this complex (Fig. 5a) that was previously reported⁵⁹. Given also that NA does not block formation of slip-outs from denatured repeat-containing DNAs (Fig. 1e), our data do not support a role of NA in blocking formation of slipped-DNAs either with or without MutS β . We further tested possible overlap of MutS β and NA pathways. MSH3 knock-down suppressed CAG repeat expansions in cells, confirming the essential role of MutS β in active repeat instability^{2,3,52,53,60}. MSH3 knockdown also blocked the effect of NA on repeat instability (Fig. 5b). Thus, NA depends upon MutS β , and its effect on inducing contractions depends upon active CAG instability.

Replication Protein A (RPA) inhibits formation of unusual DNA structures, like hairpins, by binding and stabilizing single-stranded regions^{61,62}, and enhances DNA polymerase progression through structured DNA templates^{63,64}. Polymerase delta (pol δ) is implicated in CAG repeat instability^{65,66} and active in brains in a repair capacity⁶⁷. Pol δ was unable to synthesize across a CAG tract, and this was rescued by RPA (Fig. 5c). NA competitively blocked interaction of RPA with slipped-CAG repeats (Fig. 5c) and blocked enhanced progression of pol δ along the CAG template (Fig. 5d). NA was also able to block progression of pol β (data not shown). These results support a mechanism whereby NA induces CAG contractions by blocking RPA from binding slip-outs, which would otherwise facilitate polymerases to synthesize through CAG templates (Fig. 5c). NA may disrupt the interaction or activity of other repair proteins on CAG slip-outs.

NA modulates repeat instability in the striatum of HD mice.

In HD mice and HD patients, the largest somatic CAG expansions and most neurodegeneration occur in the striatum^{1,2,14,68}. R6/2 mice harbor a single-copy transgene of *HTT* exon 1^{69,70}. R6/2 is one of the best characterized models of repeat instability, with instability patterns and tissue-specificity comparable to HD knock-in models^{1,28,71–74} and human HD patient brains^{1,7,28,73–75}. CAG expansions are evident in the striatum of these mice as early as a few weeks, which continue as the mice age¹⁴. All HD CAG mouse models assessed show a similar pattern of ongoing spontaneous CAG expansions in striatum⁷⁴, which was quantified in one model to show broadly distributed sizes of additional repeats gained at a rate of ~3.5 CAG units/month/cell^{76,77}.

Our dosing protocol involved one, two, or four stereotactic injections into the striatum of 6-week old R6/2 HD mice, each spanning a total of 4 weeks, when DNAs were harvested. Since pups of the same litter inherit different CAG lengths, each inheriting around 150–160 CAG repeats, this complicates a direct comparison of the effect of NA between mice. Instead, we injected the left striatum with NA (in saline) and the right striatum with saline only to serve as an internal control. NA intra-striatal injections led to contractions of the expanded repeat relative to the saline-only injections in the same mice (Fig. 6). In the absence of treatment, CAG length distributions between left and right halves of the striatum

for a given mouse were identical within the limits of experimental resolution. Thus, NA specifically induces CAG length differences in mice (Fig. 6a).

Continued repeat contractions resulted from additional NA administrations over a four-week period, with the most striking effect after the fourth administration. This was highly reproducible for a total of 13 mice (one for 1 injection, two for 2 injections, and ten for 4 injections; Fig. 6a, Supplementary Figs. 3–6, and Extended Data Fig. 8). NA injection did not alter brain morphology or induce cell death or cell proliferation (Extended Data Fig. 9a–c). The effect of NA was similar between mice, regardless of inherited repeat length. A bimodal distribution of repeat sizes is present in HD patient brains^{7,28,75}. The second peak of larger expansions is evident in the striatum of most CAG mouse models and was found to consist of the most vulnerable HD cells, medium spiny neurons^{1,4,68}, and to have greater levels of expanded CAG transcripts⁷⁴. NA had a greater contracting effect on the larger expansions of the bimodal repeat distribution (Fig. 6d). This portion of larger-sized expansions in the striatum may have arisen by mutation events involving large slip-outs, large enough to be bound by NA. Instability analyses in HD individuals suggests that the number of CAG units gained or lost at each mutation event are predominantly changes of one repeat unit, but may include changes of 5–15 repeat units, sizes that could be bound by NA^{78–80}. Slipped-DNAs at the DM1 locus, isolated from various tissues of DM1 patients, including brain, also presented a bimodal distribution of slip-out sizes, with peaks of ~30 and <10 repeats¹³, where the former could be bound by NA.

Most alleles in the NA-treated striatum showed contractions of CAG repeats, indicating that NA affected most cells (Fig. 6a, Supplementary Figs. 3–6, and Extended Data Fig. 8). Notably, contractions were detected by standard PCR and did not require more sensitive small-pool PCR. Hence, they were robust, seeming to occur *en masse* in most cells. We quantified the somatic “instability index”^{76,77}: higher indices reflect greater expansions, whereas lower indices reflect lower expansions or greater contractions (Extended Data Fig. 7b). The number of contracted vs. expanded peaks (Fig. 6b) or the relative composition (%) of contracted vs. expanded peaks (Fig. 6c) was greater with subsequent NA treatments. Repeat size distributions in striatum treated four times with NA were significantly different from mock saline-treated striatum (Mann-Whitney, $P = 0.00034$). The effect of NA was localized to the site of injection, as the CAG tract in cerebral cortex and cerebellum from the same mice showed identical patterns of CAG length heterogeneity between the right and left sides (Fig. 6d,e and Supplementary Figs. 3–6).

NA induced contractions rather than only arresting expansions because the peak repeat length in the NA-treated striatum was shorter than the inherited tract length in the tail of the same mouse, which remains constant throughout the mouse’s lifetime (Fig. 6d,e and Supplementary Figs. 3–6). For a given mouse, the repeat size distributions in the NA-treated half of the striatum shifted towards contraction, relative to the inherited length in the tail, while the saline-treated half continued to incur expansions (Fig. 6b–e and Supplementary Figs. 3–6; see of main peaks where saline- vs. NA-treated vs. tail CAG lengths are reduced by 4–7 CAG units). This suggests that injections of NA into the striatum induced contractions of the expanded CAG tract, and thereby countered the expansion bias in that

tissue (showing a spontaneous expansion rate of ~3.5 CAG units/month/cell, calculated as described^{76,77}).

The effect of NA *in vivo* was specific for the expanded repeat, having no effect on non-expanded repeats (Fig. 6f and Extended Data Fig. 2). Furthermore, analysis of the mouse *Hprt1* sequence in treated male mice did not show significant sequence changes in NA-treated striatum (Extended Data Fig. 3d), indicating that NA is not a general mutagen *in vivo*, but specific for CAG tracts that are actively unstable. We also performed TUNEL analyses on HD mouse striatum to determine if NA can induce DNA fragmentation and apoptosis^{81,82}. Studies with R6/2 HD mice did not show obvious TUNEL signals^{83–85}. Neither NA- nor saline-treatment (four administrations spanning four weeks) induced detectable TUNEL staining (Extended Data Fig. 9d).

To identify molecular phenotypes caused by NA-induced CAG contractions, we assessed aggregation of mutant HTT protein (mHTT) in the medium spiny neurons (MSNs) of R6/2 mice. mHTT aggregates are a key biomarker of HD: aggregation level and number of MSNs expressing aggregates are directly linked to CAG repeat length and disease progression^{86–91}. Furthermore, reductions in mHTT aggregate levels in the striatum of HD mice can increase cell viability, decrease neurodegeneration, and improve behavioral phenotypes^{92–97}. The rapid rate of mHTT aggregate turnover (~39 hours^{92,95,97}) coupled with the considerable CAG contractions induced by NA over 4 weeks (Fig. 6a) may permit detection of NA-mediated alteration of mHTT aggregate levels. To test this, we assessed the intensity of fluorescent mHTT aggregates and the number of MSN nuclei expressing aggregates in NA-treated and saline-treated striatum of R6/2 mice. The intensity of mHTT aggregates in NA-treated striatum (4 weeks), relative to the contralateral saline-treated striatum, was significantly reduced ($P = 0.0002$) (Fig. 7a,b). Furthermore, NA-treated striata also showed significant reductions (10–20%) in the number of MSNs expressing mHTT aggregates ($P < 0.0001$), with aggregates being smaller and less intense (Fig. 7a,c). Since NA does not affect transcription (Extended Data Figs. 4a and 9e) or translation of mHTT (Extended Data Fig. 4b), the reduced mHTT aggregation is most likely due to NA-induced CAG contractions and hence polyglutamine contractions arising from the contracted templates. This interpretation is consistent with the CAG/polyQ length sensitivity of mHTT aggregate formation^{86–90,98–100}. Together, these results suggest that NA can disrupt accumulation of mHTT into aggregates. Thus, NA can improve a pathological molecular phenotype by inhibiting formation of a biomarker associated with neurodegeneration and disease progression.

DISCUSSION

Targeting DNA repeats to eliminate or correct the expansion in disease cells is of interest^{2,49,101–107}, with substantial mechanistic and human data validating somatic instability as a driver of disease age-of-onset, progression and severity^{8,9,19,54,55,108,109}. Here we targeted slipped-DNA structures using a small molecule, NA, which induced contractions *in vivo* in patient cells and in the striatum of HD mice. Targeting this DNA intermediate permitted high specificity for the actively unstable mutant allele and limited off-target effects. There are many paths by which repeat instability can arise, and various

ways through which NA may act, all of which involve slipped-DNAs^{3,4,13}. Our data show that the effect of NA on CAG instability is independent of proliferation/replication, yet dependent upon transcription through the repeat (Fig. 4d,e), consistent with the reported enhanced CAG instability upon transcription²⁰. Involvement of slipped-DNAs in NA's mechanism of action is supported by their existence in patient cells at disease loci¹³, the ability to form slipped-DNAs during transcription across repeats and through R-loop processing^{17,21}, and NA's ability to block repair of slipped-DNAs (Fig. 2b).

We propose a mechanism by which NA enhances contractions of expanded repeats, while an expansion bias spontaneously arises in the absence of NA (Fig. 8). When *HTT* is transcribed along the coding CTG DNA strand, the non-coding CAG DNA strand is displaced as single-stranded, which is extended and stabilized through formation of an R-loop. Upon removal of RNA from the R-loop, which can occur in the presence of NA (Extended Data Fig. 3), slipped-DNAs can arise on both strands^{17,21}. Evidence suggests that MutS β facilitates formation of slipped-DNAs by binding to repeats^{21,56,58,110}, even in the presence of NA (Fig. 5a). To resolve these slipped-DNAs, transcription-coupled repair will be directed to the coding strand¹¹¹, which in *HTT* is the CTG strand, using the displaced non-coding CAG strand as a template for repair. Correct repair of both slip-outs would leave the tract length stable, with removal of the CTG slip-out and retention of the CAG hairpin. Repair of the CTG slip-outs *in vitro* is less efficient than repair of CAG slip-outs^{22,27,56,57,112}; therefore CTG slip-outs will often be retained, leading to an expansion bias. Repair would be facilitated by RPA-melting of slip-outs^{62,65} and RPA-enhanced polymerase gap-filling across the repeat^{61,62} (Fig. 5d). Thus, in the absence of NA, spontaneous mutations would lead to expansions. In contrast, NA-binding will drive most of the transcriptionally displaced CAG repeats into long hairpins, essentially increasing the size and number of repeat units forming the NA-bound CAG slip-outs, which may be enhanced by MutS β binding. The poor ability of RPA to melt the NA-bound CAG slip-outs would block the ability of polymerases to gap-fill¹¹³ (Fig. 5c), and ultimately block repair of NA-bound CAG slip-outs, leading to a contraction bias. Since NA bound more CAG repeats than were displaced from the CTG strand, this leads to fewer repeats incorporated in the repair product and hence contractions. That NA targets active repeat expansions is consistent with its increased efficacy in striatum over cultured fibroblasts, where the former displays higher levels of spontaneous expansions. That NA binds to and inhibits repair of long, but not short, CAG slip-outs is consistent with NA preferentially affecting repeats in striatum, which undergo large saltatory expansions (Fig. 6).

NA efficiently induced contractions of expanded CAG repeats in most striatal cells, a tissue in HD individuals that shows selective neuronal vulnerability. Our findings over a four-week period of NA treatment in mice with ~150 CAG repeats shows that neurons *en masse* incurred contractions of approximately ~0.5 repeats lost/week^{76,77}. Repeated administration led to continued contractions. Extrapolating this to an HD-affected human, we speculate that applying a drug like NA prior to rapid onset of somatic CAG expansions could effectively block expansions and induce contractions of the inherited expanded allele to shorter lengths, where treatments spanning one year could be estimated to contract the repeat by 5–25 repeats. For an HD allele of 36–70 repeats, such changes could be clinically relevant.

Mutant HTT-polyQ inclusions are biomarkers of Huntington's disease, where inclusion size and numbers of neurons expressing inclusions are directly linked to CAG repeat length and disease progression^{86–91}. Reducing levels of mHTT-polyQ aggregates in striatum of HD mice can increase cell viability, decrease neurodegeneration, and improve behavioral phenotypes^{92–97}. Complete ablation of somatic CAG expansions (but no induced contractions) caused by genetic knock-out of *MSH2*, *MSH3*, or *MLH1* delayed the detectable formation of mHTT-polyQ aggregates^{114,115}. This effect was detectable after repair-deficient mice with (CAG)110–117 had lived 5–10 months without any somatic CAG expansions. Our treatment of mice with NA for only 4 weeks was able to induce CAG contractions, and reduced both the size and frequency of mHTT-aggregates in medium spiny neurons (Fig. 7), the cells in which NA is most effective in reducing CAG expansions (Fig. 6a).

Other approaches have been used to target expanded repeats *in vivo*. Targeting the HD locus has a history that predates discovery of the *HTT* gene or the disease-causing mutation¹¹⁶. CRISPR/Cas9 targeting of the mutant *HTT* allele in HD cells deleted ~44 kb DNA spanning the promoter region, transcription start site, and CAG expansion, resulting in haploinsufficiency with a functional non-mutant allele¹¹⁰. A study using the CRISPR/Cas9 nickase that produced single strand nicks within a transgenic repeat led to contractions of the repeat in an artificial selectable cell model¹⁰⁵. Extension to an endogenous disease locus in cells or relevant tissues has yet to be demonstrated. CRISPR/Cas9 targeting only the expanded repeats at a disease locus proved not possible due to the absence of suitable PAM sequences and a likelihood of targeting other CAG/CTG repeats elsewhere in the genome. Inactivation of mutant *HTT* resulting in haploinsufficiency is possible^{102–104}. Preferential targeting of fully duplexed expanded repeats by zinc-finger nucleases¹¹⁷ or zinc-finger repressors¹¹⁸ has been demonstrated. A small molecule approach may overcome some of the *in vivo* hurdles of enzyme-mediated paths (delivery, editing efficiency, persistent nuclease/off-targets, immune response, haploinsufficiency, etc.)^{107,119–121}. Previous studies using cell models of CAG/CTG instability demonstrated that exogenously added compounds, including DNA damaging agents, can modulate repeat instability¹²². However, these compounds lack specificity for expanded repeats, and would induce mutations in non-mutant alleles and throughout the genome¹²³. In a separate strategy, a (CAG)₆ antisense oligonucleotide was able to reduce CAG expansions, but did not induce contractions of an expanded repeat⁴⁹. A mitochondria-directed compound, XJB-5–131, by unknown processes, mildly suppressed CAG expansions rather than inducing contractions¹²⁴. Similarly, an inhibitor of histone deacetylase 3 suppressed somatic CAG expansions through unknown processes¹⁰⁶. A sequence-specific polyamide directed to the fully paired duplex GAA/TTC repeat that is expanded in Friedreich's ataxia patients prevented triple-stranded structure formation and suppressed GAA repeat expansions in FRDA cells, but did not induce contractions¹⁰⁷. The earliest non-enzymatic chemical approaches to target the HD locus aimed to modulate gene regulation using ligands targeted to fully paired duplex DNAs^{116,125}.

In contrast, NA, through rational design, targets the unusual DNA structures formed by CAG repeats that are actively unstable, and can induce *en masse* repeat contractions rather than only suppressing expansions. Moreover, NA is specific for the mutant HD allele in a disease

vulnerable brain region. These attributes of NA – its specificity for CAG repeat slipped-DNA structures, its preferential effect on disease-causing expanded repeats, and its ability to induce contractions *in vivo* in an affected brain region – make it a first-in-class example showing the potential of small molecule DNA-binding compounds to impact somatic CAG repeat instability. Administration of such small molecules, once optimized for therapy, to human brains might effectively target the root cause of repeat expansion diseases and address downstream deleterious effects.

METHODS

NA synthesis is described in the Supplementary Note.

Cell culture.

Construction of the HT1080-(CAG)850 cell model was previously described²⁰. The HT1080 model cells, the HD primary fibroblasts, GM09197 (Coriell Biorepository) with (CAG)180/21⁵, and the HD primary fibroblasts, GM02191 (Coriell Biorepository) with (CAG)43/19, were cultured at 37 °C with 5% CO₂ in DMEM supplemented with 10% fetal bovine serum. Cells were treated with or without continuous exposure to 50 μM NA for 30 days (HT1080 cells) or for 40 days (primary fibroblasts). WST-1 assay was performed according to the manufacturer's instructions (Roche). All cell lines were tested to be mycoplasma-free. We performed three independent experiments for each cell line.

Proliferation of HT1080-(CAG)850 cells was inhibited by treatment with 0.5 μM Palbociclib, as described¹²⁶. Degree of proliferation arrest was assessed in living cells by counting BrdU-positive cells after 24 h incubation with BrdU in proliferating or Palbociclib-treated HT1080-(CAG)850 cells. Sustained knockdown of MSH3 by siRNA was as described⁶⁹.

Microscopy.

HT1080-(CAG)850 cells were incubated with 50 μM NBD-labeled NA for 48 h and Cell Light Plasma Membrane-RFP, BacMam 2.0 (Life Technologies, Cat # C10608), then fixed for 15 min at room temperature with 4% paraformaldehyde and washed twice for 10 min in PBS. Cells were mounted with Vectashield hard-set mounting media that contains DAPI (Vector Laboratories, Cat #: H-1500). Fluorescence images were obtained using Olympus FV1000D confocal laser scanning microscope (Olympus).

Repeat length analysis.

The (CTG)•(CAG) repeats were sized by small-pool PCR (spPCR) with the input of 1.4–1.7 genome equivalents, followed by Southern blot²⁰. Repeat size differences in models is at most 3,000 bp; therefore, being strictly conservative, a bias to amplifying shorter alleles can be possible even under optimized PCR conditions in our study. For HD primary fibroblasts, spPCR and Southern blots were performed as described²⁰ where DNA was diluted to 1.0–1.6 genome equivalents. Amplified products (PCR primers, Supplementary Table 2) were detected by Southern blot using a DIG-labeled (CAG)7 locked nucleic acid probe¹²⁷. We analyzed at least 50 alleles for each of the three experiment (more than 150 alleles/

experiment). Repeat analyses are summarized in Supplementary Table 1. The “% of repeat population” was calculated by determining the proportion of >50 individual spPCR reactions across the CAG repeat tract that harbored a certain size of repeat product¹⁸. A χ^2 -test was performed to compare the frequencies of expanded, unchanged, and contracted alleles in each set of experiments^{20,49}. The trinucleotide and dinucleotide tract lengths of the *HTT*, *CASK*, *ATXN8*, *Mfd15*, *TBP*, and mouse *Mapkap1*, *Fgd4*, and *Tbp* loci were PCR amplified (primers listed in Supplementary Table 2) following amplification conditions described elsewhere^{30,31,128–132}. Human *TBPCAG* length variability was assessed by spPCR.

mRNA quantification.

RNA was harvested using the RNeasy Plus Micro Kit (Qiagen). Total RNA was primed with random hexamers and reverse transcribed with Superscript III (Life Technologies), followed by RNaseH-treatment. Quantitative reverse transcription (RT)–PCR was performed using TaqMan Gene Expression assays or PrimeTime qPCR assays on an ABI PRISM 7900HT (Life Technologies). Level of transgene-derived mRNA was normalized to *18S* rRNA. Results were statistically analyzed using paired *t*-test. Primer sequences are listed in Supplementary Table 2.

Western blot analysis.

Lysates were prepared from HD patient fibroblasts in RIPA buffer. 20 μ g of lysate was electrophoresed at 100 V for 4 h at room temperature in 1x MOPS buffer (Thermo Fisher Scientific, Cat #NP0001) in 3–8% Tris-Acetate pre-cast protein gel (Invitrogen, Cat #EA0375BOX), transferred to PVDF Western Blotting Membranes (Sigma-Aldrich, Cat #3010040001) overnight at 4 °C at a constant voltage of 20 V. Membranes were blocked in 10% milk in TBS + 0.1% Tween-20 (TBST), incubated with primary antibody at room temperature for 2 h, and with secondary antibody at room temperature for 1 h, and then detected with ECL (GE Healthcare, Cat #RPN2232). Primary antibodies: Anti-Huntingtin Protein Antibody a.a. 181–810 Clone 1HU-4C8 (1:1,000, mouse) (Millipore Sigma, Cat #MAB2166), Anti-Actin Protein Antibody (C4 clone, 1:30,000, mouse) (BD Transduction, Cat #612657). Secondary antibodies: Peroxidase-AffiniPure Sheep Anti-Mouse IgG H+L (1:2,000) (Cedarlane Labs, Cat #515-035-062).

NA-DNA binding.

Homoduplex slipped structures of 50 repeats and heteroduplex with long (CAG)₂₀ or (CTG)₂₀ slip-outs were formed by alkaline denaturation/renaturation, as described¹⁶. Briefly, plasmids containing human DM1 genomic (CTG)_n•(CAG)_n repeats (*n* = 30 or 50) were linearized by *HindIII* digestion. DNAs of (CAG)₅₀ and (CTG)₃₀ repeats, or DNAs of (CAG)₃₀ and (CTG)₅₀ repeats, were mixed in equimolar amounts and then heteroduplexed by alkaline denaturation/renaturation. Repeat-containing fragments were released by *EcoRI* digestion and electrophoretically resolved on a 4% polyacrylamide gel. Gel-purified fragments were radiolabeled with [α -³²P]dNTPs on both strands by fill-in reaction, radioactivity of each structure was determined using Cerenkov counting, and an equivalent radioactive concentration of each structure was incubated with increasing concentration of NA for 30 min at room temperature with 1x hypotonic buffer. Binding products were

resolved by electrophoresis on a 4% (w/v) polyacrylamide gel in 1x TBE buffer at a constant 200 V for 2.5 h.

Replication assay.

In vitro replication templates containing (CTG)₇₉•(CAG)₇₉ were previously described^{133,134}. The SV40-origin of bidirectional replication was placed 103 or 98 bp 5' or 3' of the CAG repeat for pDM79EF and pDM79HF, respectively. These templates and an SV40-ori template with no-repeats (pKN16) were replicated *in vitro* by HeLa cell extract adding [α -³²P]dCTP and T-Antigen, as described^{133,134}. Replication was performed in presence or absence of NA (7.5 μ M or 15 μ M). Radioactive replication products were purified, linearized (*Bam*HI) and treated with *Dpn*I. Equal amounts of unreplicated pKN16 DNA was treated with *Dpn*I to show the complete digestion of unreplicated plasmid DNA. Equal quantities of reaction products were resolved by electrophoresis on a 15-cm 1% agarose gel run for 16 h at 4 V/cm in TBE buffer, dried, and exposed to Kodak film.

Repair assay.

To determine the effect of NA binding upon slipped-DNA repair, a series of circular slipped-DNA substrates were prepared with an excess of repeats with a nick located 5' or 3' of the slip-out^{22,56}. G-T mismatched substrate was prepared as described^{22,56}. All DNA substrates were processed *in vitro* by HeLa extracts. Analysis of repair products was performed by Southern blotting, comparing with starting material. Each repair assay has been performed in three independent experiments.

R-loop formation and processing.

Plasmids bearing (CAG)₇₉•(CTG)₇₉ tract with convergent T3 and T7 RNA polymerase promoters were described^{17,135}. Transcription reactions were performed as described¹⁷. Briefly, 500 ng of template DNA in 1x transcription buffer (Roche) and 1x bovine serum albumin (New England Biolabs) were mixed for 1 h with 20 U of the appropriate RNA polymerase: T7, T3 or T7+T3 (Roche), with or without NA 120 μ M. Products were purified and treated with either 1 g of RNaseA (Roche) alone or mixed with 1 U of *E. coli* RNaseH (Roche), at room temperature for 30 min, in presence or absence of NA 120 μ M. All *in vitro* transcription reaction products were analyzed on 1% agarose gels run in 1x TBE buffer at 80 V for 3 h. Gel-borne products were visualized with ethidium bromide (0.5 mg/ml) under ultraviolet (UV) light.

R-loop templates prepared from *in vitro* transcription and RNaseA treatments were incubated with NA and then processed by extracts of HeLa or SH-SY5Y neuroblastoma cells, where the latter were terminally differentiated by retinoic acid⁵⁶. Nucleic acids were purified and transformed into bacteria for STRIP analysis as described¹⁷. Briefly, products of human cell extract processing were transformed into *E. coli* XL1-MutS (Agilent). Individual bacterial colonies (each representing one processed template) were picked and cultured for 6 h. Magnitudes of repeat length changes were determined by electrophoretic sizing of the repeat-containing fragments on 4% polyacrylamide gels relative to the starting length material and a size marker. Data are derived from three independent *in vitro* transcription and human cell extract processing reactions with ~150 colonies (~50 colonies

per replicate) representing 150 individual products of cell extract treatment analyzed for each R-loop configuration. Individual experiments were compared using the χ^2 -test.

MutS β binding assay.

MutS β was purified from baculovirus-infected Sf9 cells expressing His-tagged hMSH2 and hMSH3 as described²². Binding reactions were performed at room temperature. Slipped-DNA with long (CAG)₂₀ was prepared and end-labeled as described above. Protein was incubated with DNA for 30 min in a buffer containing 10 mM HEPES-KOH pH 7.5, 110 mM KCl, 1 mM EDTA, and 1 mM DTT with or without ATP in the buffer, as indicated. Reactions were loaded onto a 4% native polyacrylamide gel with non-denaturing loading dye (20 mM Tris-HCl pH 7.4, 4% glycerol, bromophenol blue). Gel was run in 1x TBE buffer for 2 h.

Mung bean nuclease footprinting.

Experimental conditions used were single-hit kinetics, as described¹⁶.

RPA DNA-binding.

Recombinant RPA protein was expressed in BL21(DE3) cells and binding was performed as described¹³⁶.

Polymerase extension assay.

Recombinant human polymerase δ (pol δ) was prepared in insect cells using a baculovirus vector and purified by immunoaffinity column chromatography, as described¹³⁷. Pol δ extension assay was performed as described¹³⁸, using an oligo containing (CAG)₁₀ repeats, as described²⁴. Briefly, 0.1 μ M primer and 0.1 μ M oligo were denatured at 95 °C for 3 min, annealed for 30 min at room temperature, and incubated with NA for 30 min at room temperature. RPA and/or pol δ were added and the reactions was started by adding 0.1 mM dNTPs in 10 μ l reaction volume, and incubated at 37 °C for 15 min. The reaction was stopped by adding 20 mM EDTA and purified by extraction with phenol/chloroform/isoamyl alcohol (25:24:1, v/v/v) followed by ethanol precipitation. Pellets were resuspended in formamide buffer, denatured at 95 °C for 10 min, and run on a 6% sequencing gel at 2,000 V and 90 W for 40 min.

Stereotaxic injections into R6/2 mice.

Mouse handling and experimental procedures were conducted in accordance with the Osaka University guidelines for the welfare of animals. A single NA application involved six separate stereotactic injections (three injections of NA or saline into three different striatal regions of either the left or right striatum, respectively). Under sterile conditions, six male R6/2 mice (B6CBA-Tg(HDexon1)62Gpb/1J, Jackson Laboratory, cat# 002810), 6-week-old, were anesthetized with 50 mg/kg pentobarbital sodium, and stereotactically injected with 5 μ L of saline (PBS solution) (right side) or 500 μ M NA dissolved in saline (left side). The control for NA-treatment is therefore the contralateral side of the striatum of each mouse. Mice received injections once or twice bi-weekly, or weekly for 4 consecutive weeks. Stereotaxic injections were delivered to three sites within the striatum with the following

coordinates: (anterior-posterior (AP) = 0.0 mm, medial-lateral (ML) = 1.5 mm from bregma, dorsal-ventral (DV) = 2.5 mm below the dural surface; AP = 1.0 mm, ML = 1.5 mm, DV = 2.5 mm; and AP = 0.5 mm, ML = 1.5 mm, DV = 2.5 mm), using a 10- μ l Hamilton microsyringe at a rate of 0.5- μ L/min. Both right and left striatum were assessed for repeat length at the HD CAG transgene and at endogenous CAG tracts. For the mice treated four times, DNAs from the tail prior to and following NA administration, as well as left and right frontal cortex and cerebellum, were harvested. Coronal sections of the striatum were cut serially at 20 μ m thickness using a cryostat (CM1850UV; Leica Microsystems). Striatum sections of 0.62, 1.10, and 1.58 mm posterior from bregma were washed in PBS containing 0.05% Triton X-100 (PBS-T). They were then immersed in a solution of 3% H₂O₂, 10% methanol in PBS for 10 min. After washing 3 times with PBS-T, the sections were incubated with primary antibody (mouse anti-NeuN, 1:100, Millipore Bedford, MA; rabbit anti-doublecortin, 1:200, Abcam,) diluted in blocking solution of 10% Block-Ace blocking solution (Yukijirushi Co.) overnight at 4 °C and then with biotinylated secondary antibody (1:500, VECTOR Laboratories) in PBS-T for 1 h at room temperature followed by VECTASTAIN ABC reagents (1:100, VECTOR Laboratories) in PBS for 1 h at room temperature. The sections were washed 3 times with PBS-T in between the steps. The bound complex was visualized with 3,3'-diaminobenzidine (Sigma).

Genescan analysis.

At 4 weeks after the first injection, DNA was isolated from mouse brain tissue as described¹²⁷. PCR was performed as described previously¹³⁹, and PCR products were sized on an ABI310 Gene Analyser using GENESCAN 3.1 software (Life Technologies).

Instability Index calculation.

Instability index was calculated as described^{76,77} with modifications as outlined in Extended Data Figure 7.

Immunofluorescence.

Medium spiny neuron (MSN) specific mutant HTT aggregates were assessed using a multiplexed immunofluorescence approach staining for HTT protein (EM48 antibody, cat.# MAB5374, Millipore-Sigma) and anti-DARPP-32 (19A3 antibody, cat.# 2306S, New England Biolabs - expressed almost exclusively by striatal medium spiny neurons), as described¹⁴⁰. After rehydration, slides were subjected to antigen retrieval in 10 mM sodium citrate for 20 min in a steamer and cooled to room temperature for 1 h. Slides were washed twice in 1x PBS + 0.05% Tween-20 (1x PBST) (2 min, 2 times). Slides were blocked in 10% normal goat serum for 1 h at room temperature and incubated with primary antibody overnight at 4 °C. Secondary antibody incubation was performed for 1 h at room temperature. Slides were mounted with Hardset VectaShield with DAPI. Aggregates were then blindly assessed in two ways:

1. Whole striatal assessment of red pixel intensity (mHTT aggregates) via ImageJ. Intensity was measured from 20x images obtained via a 3DHitech Panoramic 250 Flash II Slide Scanner. Each individual striatal intensity per slice was normalized to the total striatal intensity of the slice and then plotted. Three

separate brain slices were assessed per mouse, assessing a total of 4 mice (each treated 4 times over 4 weeks).

2. Counting MSN nuclei containing mHTT aggregates from confocal images obtained from a Quorum Spinning Disk Confocal (Olympus IX81 microscope). Ten 40x (water) confocal images were taken at 10 different locations per striatum with ~100 cells per image (~1,000 cells per striatum, or ~2,000 cells total per brain slice) being assessed. 3 striatal slices were assessed per mouse (4 mice total, ~3,000 cells assessed per striatum per mouse). Percentages of cells containing mHTT aggregates were taken relative to the total number of cells in the image.

Whole-genome sequencing, alignment, and variant calling.

WGS was performed using established protocols on Illumina instruments and paired-end FASTQ files were aligned to the human genome (hg19/GRCh37) using BWA-MEM (v.0.7.8), with Picard MarkDuplicates (v.1.108) being used to mark PCR duplicates. Indel realignment and base quality scores were recalibrated using the Genome Analysis Toolkit (v.2.8.1). Somatic mutations were detected using MuTect2 (part of GATK v.3.5)¹⁴¹. Mutations present only in treated cells (as opposed to non-treated cells) were retained. For substitutions, we also removed common single-nucleotide polymorphisms (SNPs) as described⁴⁴. To remove common germline variants, we used an in-house panel of controls and removed any putative substitutions present in 2 controls. Putative substitutions were also removed if they were overlapped with a highly repetitive sequence (using DUST¹⁴² with score > 60) or were located in excessively high-depth alignments in difficult to align regions of the genome, as described¹⁴³. We apply a maximum depth threshold of $d + 4\sqrt{d}$, where d is the average normal mean read depth of the chromosome in the corresponding untreated cell.

Mutational signatures shown in COSMIC, were screened for using a further elaborated version (v0.0.5.75⁴⁰) of an established nonnegative matrix factorization-based method, SigProfiler^{144–146}. This framework works in two steps: (1) *de novo* extraction of signatures on the catalogue of substitutions using non-negative matrix factorization approach; and (2) comparing deciphered *de novo* signatures to a set of previously described mutational signatures (COSMIC Mutational Signatures v3) using cosine similarity to identify the etiology of the underlying mutagenic process. It is common practice to only consider mutational signatures with >100 mutations as reliable.

HPRT1 sequence analysis by SMRT-CCS sequencing.

DNAs were extracted from three independent NA- or saline-treatments of the HD primary fibroblasts (GM09197) and three independent NA-treated and control striata of three R6/2 mice. Details of the sequencing results are described in the Supplementary Note. Mutation rates were not significantly different between NA- and saline- sequences (two-sample Kolmogorov-Smirnov test).

Microsatellite instability assay.

Microsatellite instability was assessed as per Gallon *et al.*³². Briefly, >20 mononucleotide repeats were amplified from 50 ng of template DNA using single molecule molecular inversion probes, and sequenced to a median (Q1-Q3) depth of 1,007 (733–1,515) reads/ marker/sample using a MiSeq (Illumina). Sequencing reads were aligned to the human reference genome (build hg19) using BWA¹⁴⁷. Frequencies of microsatellite length variants were extracted for each marker in each sample, and converted to a probability by comparison to a reference distribution generated from 40 microsatellite stable, peripheral blood leukocyte controls. A sample score is calculated by combining probabilities from each marker using Fisher's method, and multiplying the decadic logarithm of this combined probability by –1. Scores >1.3 are therefore equivalent to a >95% probability that the observed frequency of microsatellite length variants for a sample is greater than the reference set, and is used as a classification threshold. Residual samples from Gallon *et al.*³², comprising peripheral blood leukocyte DNA of 3 constitutional mismatch repair deficiency and 8 control patients, were used as controls.

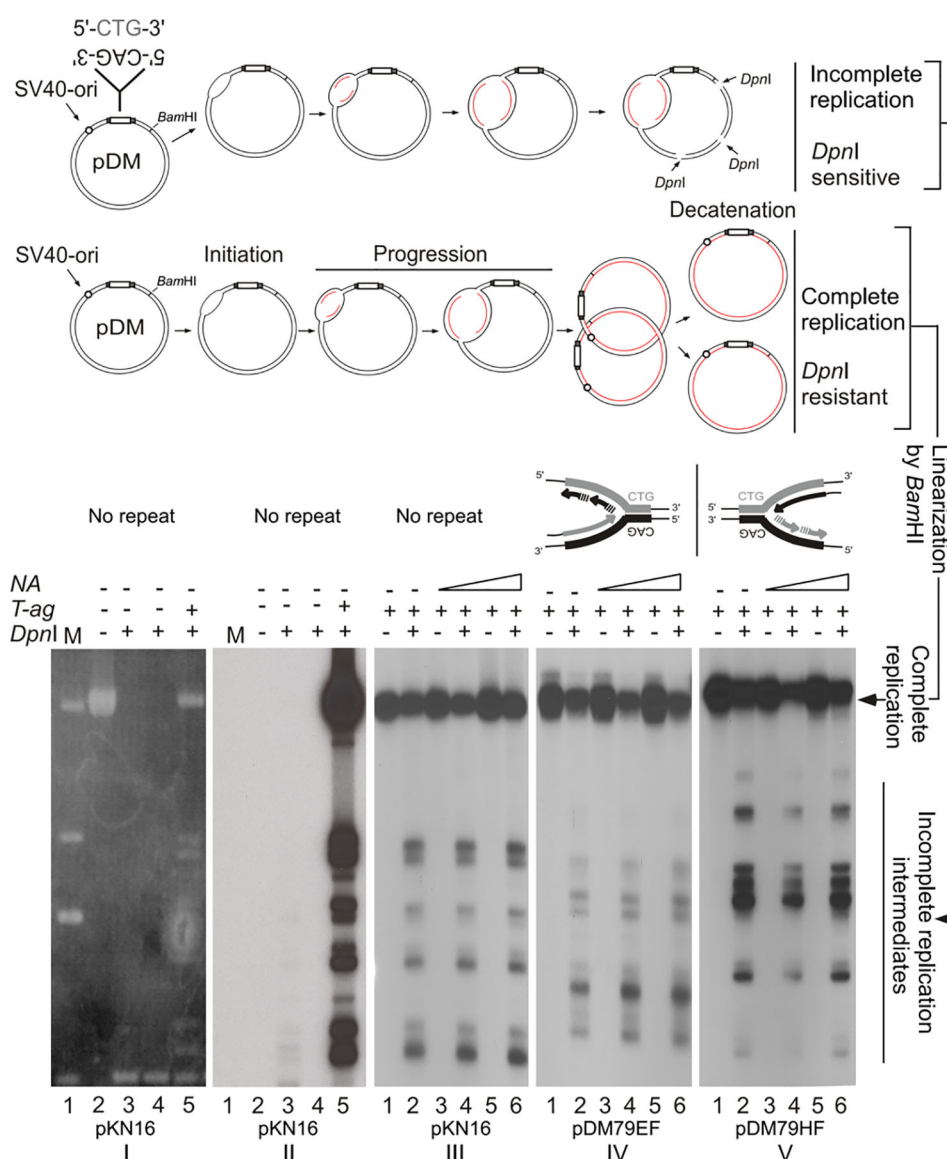
TUNEL assay.

TUNEL assay was conducted using the Click-iTTM Plus TUNEL Assay for In Situ Apoptosis Detection, Alexa FluorTM 488 dye (Invitrogen, cat #: C10617), multiplexed with anti-DARPP-32 (19A3 antibody, cat.# 2306S, New England Biolabs), as outlined by the manufacturer.

DATA AVAILABILITY STATEMENT

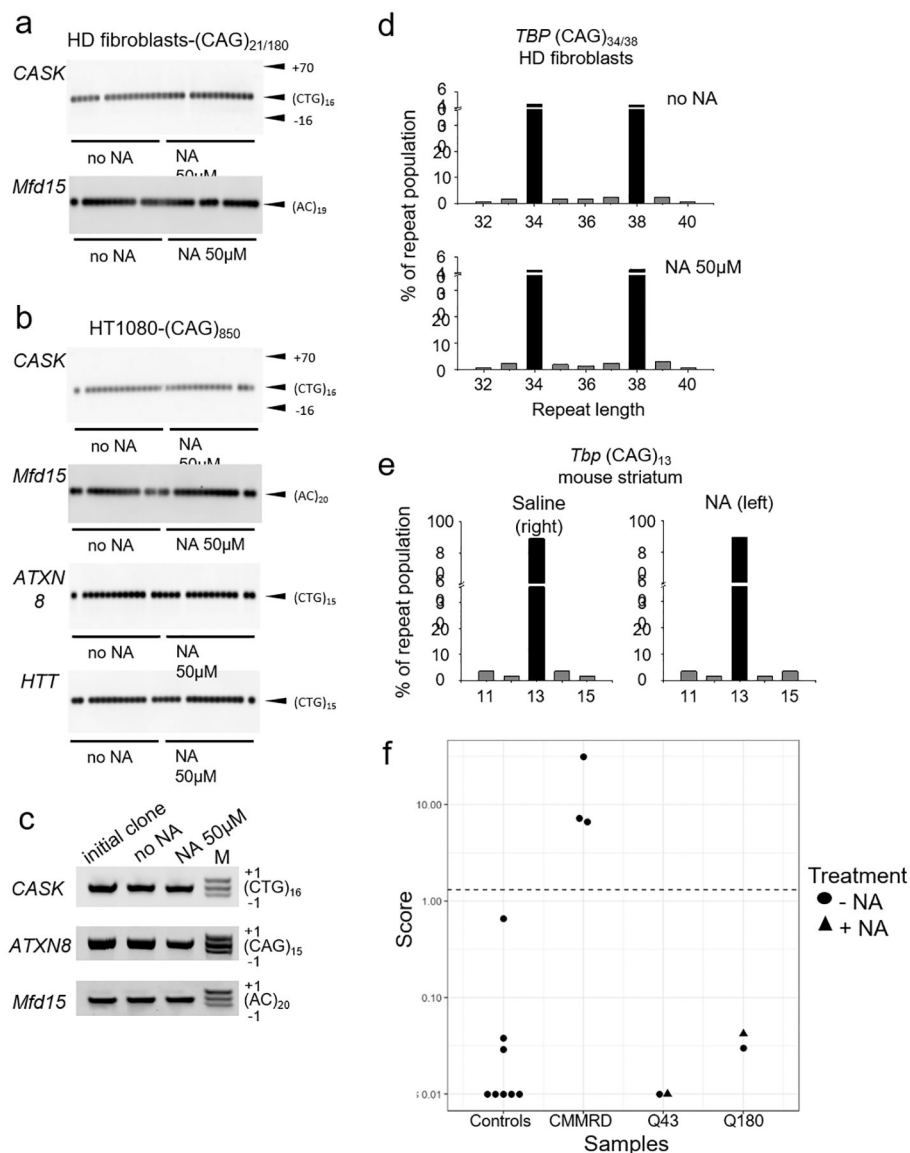
Raw sequencing data have been deposited at the Sequence Read Archive (SRA) under accession number SUB6615083.

Extended Data



Extended Data Fig. 1. NA does not affect replication efficiency or replication fork progression
 Three circular plasmids containing the SV40 origin of replication, and an expanded (CAG)₇₉•(CTG)₇₉ repeat tract (pDM79EF and pDM79HF) or no repeats (pKN16), were replicated *in vitro* by human (HeLa) cell extracts without or with NA (7.5 μ M or 15 μ M) treatment. The location of SV40-ori determines the replication direction and which strand will be used as the leading or the lagging strand template. pDM79HF uses the CAG strand as the lagging strand template, while pDM79EF uses the CTG strand as the lagging strand template (schematic on the top of the gel panel). Replication products were purified and linearized with *Bam*HI. An equal portion of the reaction material was also digested with *Bam*HI and *Dpn*I as *Dpn*I digests un-replicated and partially-replicated material, as shown in the schematic (top figure). The digestion products were electrophoresed on a 1% agarose gel to resolve completely replicated and un-replicated material (bottom figure). Equal amount of unreplicated plasmid DNA was digested with *Dpn*I and stained with Ethidium Bromide to

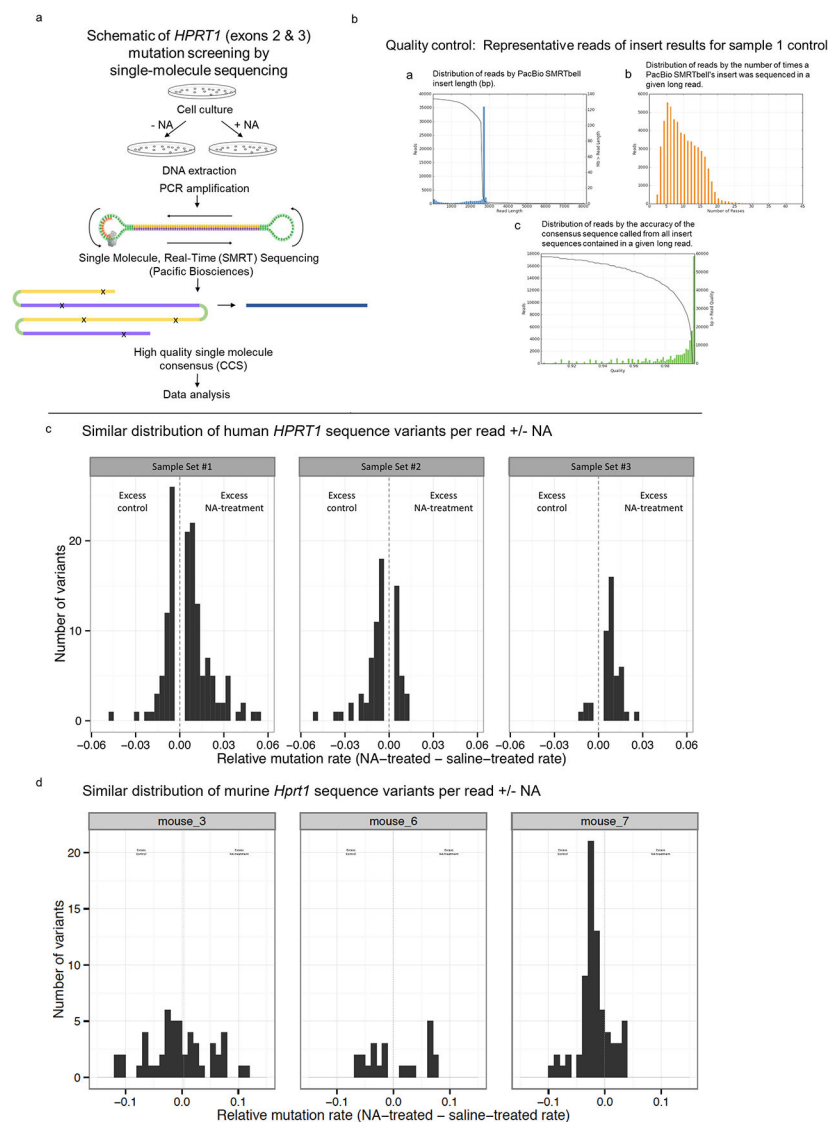
show the complete digestion of unreplicated plasmid DNA (Bottom panel). Panel I, ethidium bromide stained, Panel II, autorad: marker (lane 1); *DpnI* undigested plasmid DNA (lane 2); *DpnI* digested unreplicated plasmid DNA (lane 3–4); replicated plasmid DNA, *DpnI* resistant (lane 5). No difference in *DpnI* resistant material is observed between replication in the presence or absence of NA, in all the three templates tested (panel III, IV, V). Blots have been cropped and the corresponding full blots are available in the Source Data files.



Extended Data Fig. 2. NA does not affect non-mutant genetically stable repeats

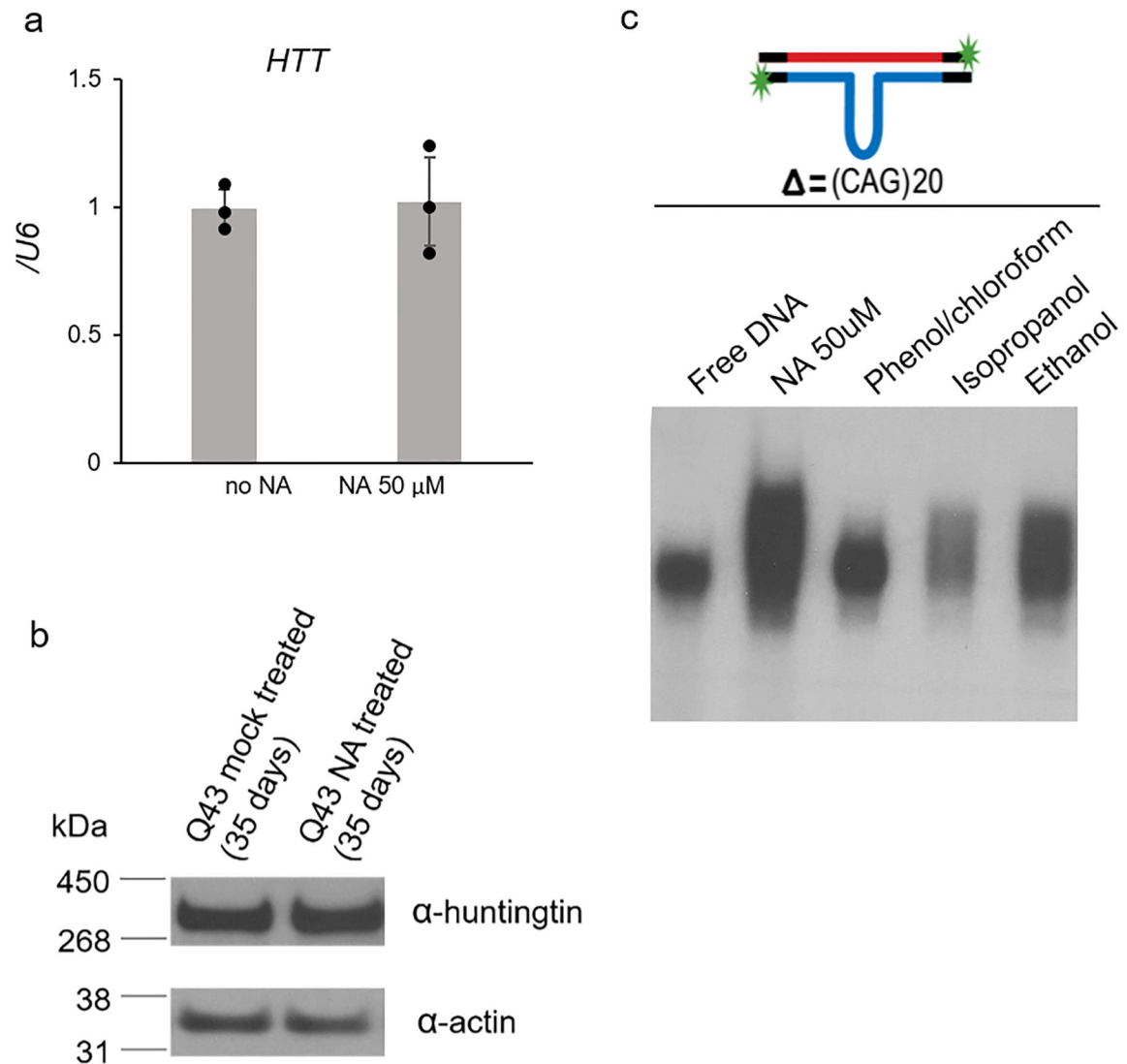
a,b, Representative data showing small-pool PCR for the non-expanded CAG/CTG repeat length of *CASK* and *Mfd15* in HD primary fibroblast cells (**a**) and small-pool PCR for the non-expanded CAG/CTG repeat length of *CASK*, *Mfd15*, *ATXN8* and the non-expanded *HTT* allele genes in HT1080-(CAG)₈₅₀ cells (**b**). Even under the sensitive mutation detection capacity of spPCR, length variation was not observed in either NA treated- and untreated-cells. Notably, some reactions did not show any product as is typical of the low genomic DNA template dilutions used in small-pool PCR. **c**, Repeat-tract lengths of the *CASK*, *ATXN8*, and *Mfd15* loci in HT1080-(CAG)₈₅₀ cells (initial clone and cells after 30 days incubation with or without NA). Length variation was not observed at any of these repeats of normal length loci in HT1080-(CAG)₈₅₀ cells (after 30 days incubation with or without NA). Three independent experiments were performed. **d**, Small-pool PCR for the non-expanded CAG tracts in TBP alleles in HD patient fibroblasts treated with or without

NA for 40 days. **e**, Small-pool PCR for the non-expanded CAG tracts in TBP alleles in HD R6/2 mouse striatum with four injections of NA or saline. **f**, Microsatellite instability assay. Assay scores >1.3 indicate increased MSI relative to a control sample set from peripheral blood leukocytes. Both NA positive and NA negative HD cells with (CAG)43 or (CAG)180 scored <1.3, indicating no effect of treatment on MSI. 8 known CMMRD-negative controls and 3 known CMMRD-positive controls were included in the assay.

NA does not induce mutation in *HPRT1* / *Hprt1***Extended Data Fig. 3. NA is not a general mutagen**

Towards assessing whether NA-treatment acted as a general mutagen to sequences other than CAG slip-outs, we harnessed the high read accuracy and depth of single molecule, real time, circular consensus sequencing (SMRT-CCS). Single-molecule sequencing was done on the *HPRT1* gene – widely used as a surrogate indicator of the global effect of induced genetic variation. For each replicate, we calculated the relative mutation rate between NA- and saline-treated cells as the mutation rate for NA-treated cells minus the rate for saline-treated cells and identified excess mutation rates based on an absolute relative rate $>0.5\%$. **a**, Schematic of *HPRT1* sequencing for mutation detection. Briefly, cells were grown under identical conditions differing only by the addition of NA (50 μM) or saline, DNAs were isolated, *HPRT1* exons 2 and 3 PCR amplified and sequenced. **b**, Quality control for our analysis. **c,d**, Comparison of sequence variations between NA-treated and saline treated is presented. We chose to compare the single-molecule sequence reads of individual X

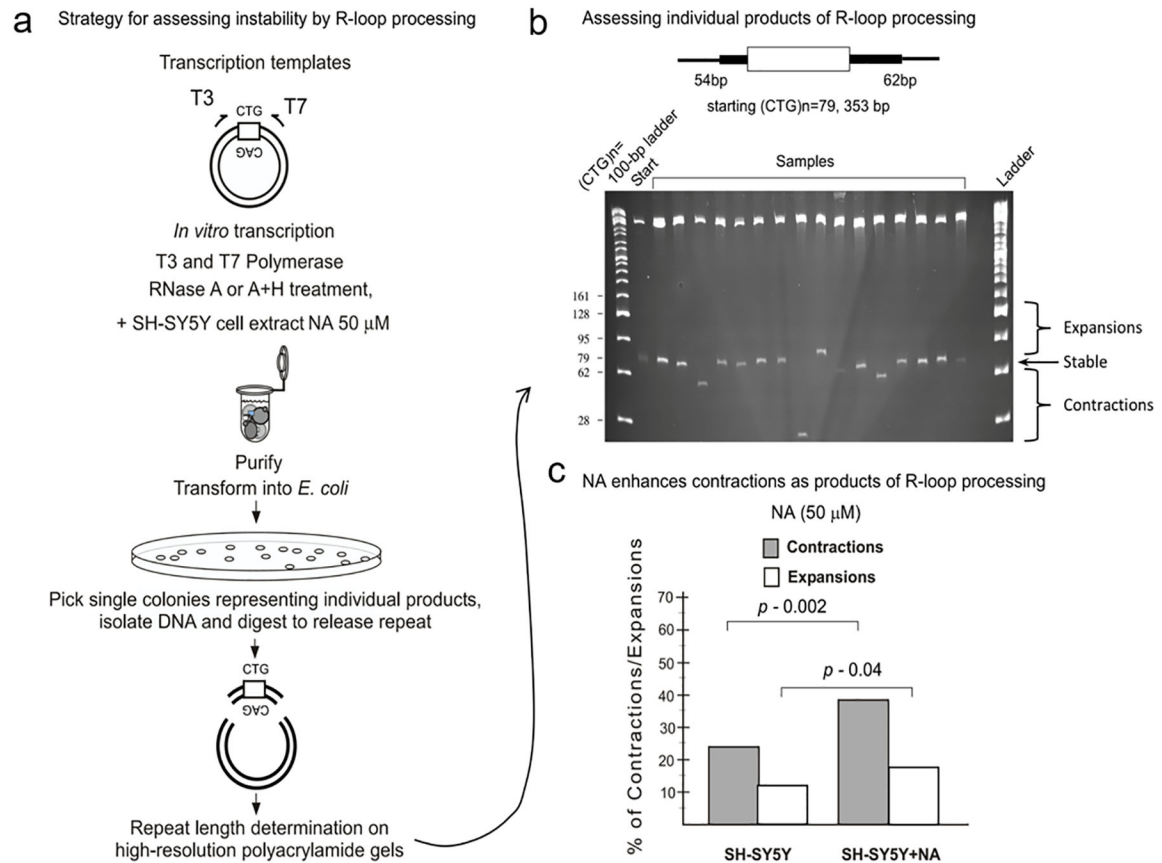
chromosome-linked *HPRT1* alleles (exons 2 and 3) from our male HD patient-derived cells (c), and our male R6/2 mice (d), that had been NA- or saline-treated. Each read represents a single cell (Supplementary Note). Graphs show the distribution of sequence variants by relative mutation rate between three experimental replicates of NA-treated and saline-treated cells sequenced with PacBio single-molecule long reads.



Extended Data Fig. 4. NA does not affect HTT transcription or translation

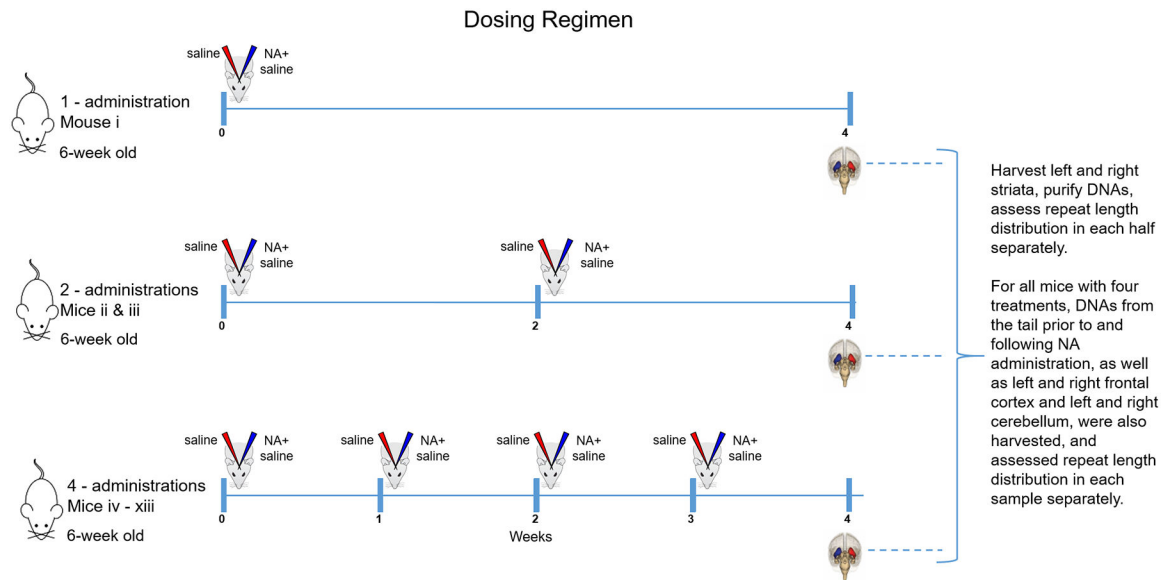
a, NA does not affect transcription across expanded repeats in HTT in HD patient cells, determined by quantitative real-time reverse transcriptase (qRT)-PCR and normalized to U6 RNA. Data are indicated as the mean \pm s.d. of independent triplicates. **b**, Western blot showing that NA does not affect HTT translation in HD patient cells with (CAG)43. Western blots were repeated 4 times with similar results. Blots have been cropped and the corresponding full blots are available in the Source Data files.

NA enhances contractions during the processing of R-Loops



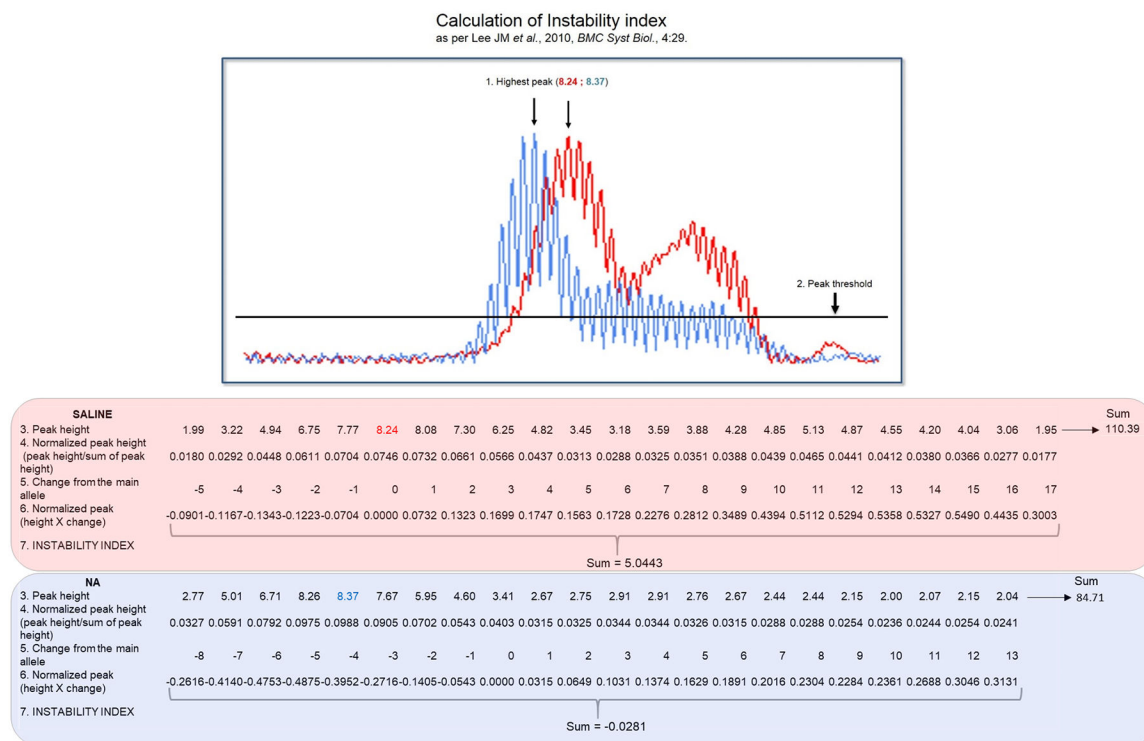
Extended Data Fig. 5|. NA induces contractions during R-loops processing.

a, Schematic of R-loop formation, processing, and analysis. Pre-formed double-R-loops were processed by terminally differentiated (retinoic acid) human neuron-like cell extracts (SH-SY5Y) in the absence or presence of NA (50 μ M), as described and DNA repeat lengths scored as expansions, contractions, or stable, by the STRIP assay (Methods). **b**, Representative example of STRIP analysis. Transcription products were isolated, processed and transformed in *E. coli* cells, previously shown to stably maintain the (CAG) $_{79}$ •(CTG) $_{79}$ lengths (Methods). Plasmids isolated from individual bacterial colonies were digested with restriction enzymes to release the repeat containing fragment, resolved on 4% polyacrylamide gels and scored for instability. **c**, Graphical analysis of STRIP results. Two-sided χ^2 test was performed to compare 191 untreated colonies vs. 100 NA-treated colonies.



Extended Data Fig. 6. Dosing regimen

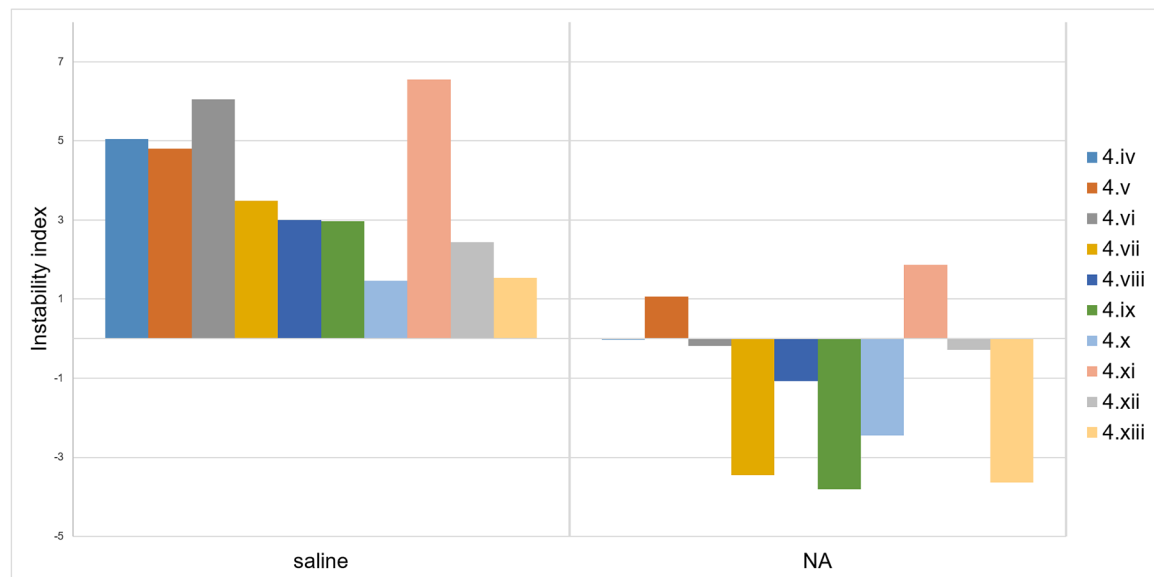
A single drug administration involved six separate stereotactic injections (three injections of drug in saline or saline into three different striatal regions of either the left or right striatum, respectively). At the onset mice were 6-weeks old.



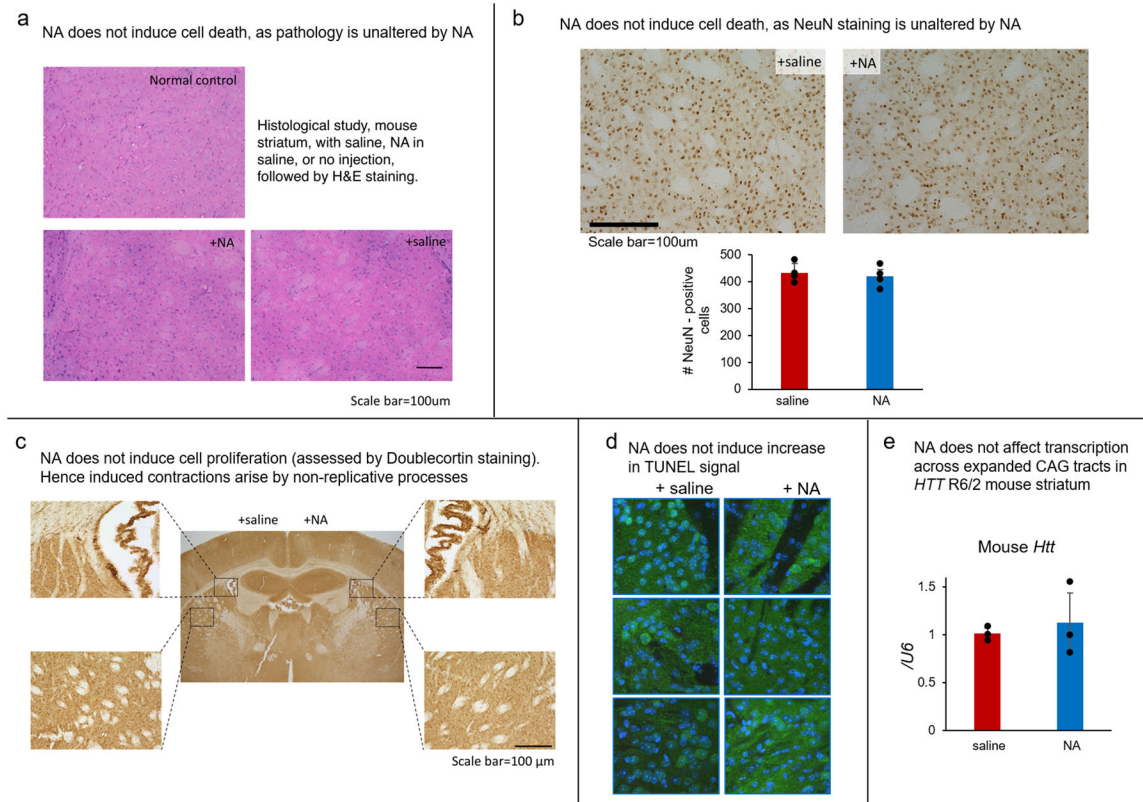
Extended Data Fig. 7. Instability Index calculation

Instability index determination was as described^{76,77}, using a relative peak height threshold, with modifications. To quantify the levels of instability from GeneMapper traces peak height was used to determine a relative threshold of 20% based upon the main peak in the shorter mode of the control striatum (see points 1 & 2 in the figure). We used a conservative threshold factor (20%) as this detects peaks with good signal intensity and is more resistant to amplification variation than lower thresholds. Lower thresholds (10%, 5%) can provide more sensitive quantification. Peaks falling below this threshold were excluded from analysis. Peak heights were scored (see point 3) and normalized to the total of all peak heights in a given scan (see point 4). Since we are comparing the effect of NA versus saline upon instability in the striatum, the CAG length distribution in tail is not a factor in this comparison, but is for determining absolute instability, as in previous studies^{61,65}. So as to facilitate comparison between NA and saline-treated striatum, these were normalized by multiplying the values by the change in CAG length of each peak relative to the highest peak in saline-treated striatum (see point 5), as opposed to the highest peak in the tail, as previously done^{76,77}. These normalized values (see point 6) were summed to generate the instability index (see point 7). Striatum analysis for mouse vi is shown as an example R6/2, 6-weeks treated with four injections spanning 4 weeks of saline (red) or NA (blue). Peaks of the main allele in the saline-treated striatum, NA-treated striatum and tail of the same mouse, are indicated by triangle-brackets at the top (see point 1).

10 mice with 4 injections of NA

**Extended Data Fig. 8. A total of ten HD mice revealed consistent NA-induced contractions of expanded CAG repeats**

Instability Indices in striatum of ten mice (iv-xiii) treated four times with saline in the right striatum and NA in the left striatum. Indices in NA-treated striatum were significantly different from the control saline-treated striatum (Mann-Whitney, $P = 0.00035$). Instability Indices for mouse v and xi are positive for both NA and saline as there are less data points to the left of the highest peak compared to the points to the right. Still, after NA treatment there is a reduction in the index.



Extended Data Fig. 9. NA does not induce cell death in the CNS and cell proliferation, and does not affect transcription across the *Htt* locus

a, Histological study, mouse striatum with saline, NA in saline, or no injection, followed by H&E staining. Three independent experiments were performed. **b**, NeuN staining showing that NA does not induce cell death. Quantification of NeuN positive cells below. Data are indicated as mean \pm s.d. of triplicates. **c**, Doublecortin staining showing that NA does not induce cell proliferation. Three independent experiments were performed. **d**, The effect of NA on TUNEL signal as assessed via fluorescent microscopy and immunohistochemistry. Representative 40x magnification confocal images of striatal medium spiny neurons (MSNs) of R6/2 mice treated with saline (left striata) and 50 μ M NA (right striata) stained for TUNEL (red, staining apoptotic cells), and DARPP32 (green, staining MSNs). Panel locations (i-vi) correspond to the locations outlined in Figure 7 (middle panels). **e**, NA does not affect transcription across expanded repeats in *HTT* in HD patient cells and mouse striatum, determined by quantitative real-time reverse transcriptase (qRT)-PCR and normalized to U6 RNA, expressed as the ratio of NA-treated vs. PBS-treated R6/2 striatum. Data are indicated as mean \pm s.d. of independent triplicates.

Supplementary Material

Refer to Web version on PubMed Central for supplementary material.

ACKNOWLEDGEMENTS

This work was partially supported by the Canadian Institutes of Health Research (FRN388879) (J.-Y.M.), (FRN148910) (C.E.P.), the Muscular Dystrophy Canada (C.E.P.), Tribute Communities (C.E.P.), The Petroff Family Fund (C.E.P.), The Kazman Family Fund (C.E.P.), The Marigold Foundation (C.E.P.), The National Center of Neurology and Psychiatry (29-4) (M.N.), a JSPS KAKENHI Grant-in-Aid for Young Scientists (Start-up) and (A) (24890110 and 25713034) (M.N.), Scientific Research (B) (16H05321) (M.N.), and Specially Promoted Research (26000007) (K.N.), Cancer Research UK Catalyst Award (C569/A24991) (R.G.), and US National Institutes of Health (2 R01 ES014737) (M.Y.W.T.L.), and a US National Institutes of Health (NIH) grant (HG010169 to E.E.E.). E.E.E. is an investigator of the Howard Hughes Medical Institute, A.S. holds the Canada Research Chair in Childhood Cancer Genomics, J.-Y.M. holds the Fonds de Recherche de Santé Québec Chair in Genome Stability, C.E.P. holds the Canada Research Chair in Disease-Associated Genome Instability. We acknowledge the technical support of Rika Manabe, Kimie Hayashi, Peixiang Wang, Lisa Yu, Mila Mirceta, Neha Thakkar, Ineka Panigrahi, David Ripsman, Hemanta Adhikary, Stéphanie Bérubé, Yan Coulombe, Anthony Couturier, Melanie Scofield Sorensen, and Kendra Hoekzema. We acknowledge TCAG (Sick Kids) for expedited sequencing.

References

- Kennedy L et al. Dramatic tissue-specific mutation length increases are an early molecular event in Huntington disease pathogenesis. *Hum Mol Genet* 12, 3359–67 (2003). [PubMed: 14570710]
- Lopez Castel A, Cleary JD & Pearson CE Repeat instability as the basis for human diseases and as a potential target for therapy. *Nat Rev Mol Cell Biol* 11, 165–70 (2010). [PubMed: 20177394]
- Mirkin SM Expandable DNA repeats and human disease. *Nature* 447, 932–40 (2007). [PubMed: 17581576]
- Pearson CE, Nichol Edamura K & Cleary JD Repeat instability: mechanisms of dynamic mutations. *Nat Rev Genet* 6, 729–42 (2005). [PubMed: 16205713]
- Sathasivam K, Amaechi I, Mangiarini L & Bates G Identification of an HD patient with a (CAG)180 repeat expansion and the propagation of highly expanded CAG repeats in lambda phage. *Hum Genet* 99, 692–5 (1997). [PubMed: 9150744]
- Morales F et al. Somatic instability of the expanded CTG triplet repeat in myotonic dystrophy type 1 is a heritable quantitative trait and modifier of disease severity. *Hum Mol Genet* 21, 3558–67 (2012). [PubMed: 22595968]
- Swami M et al. Somatic expansion of the Huntington's disease CAG repeat in the brain is associated with an earlier age of disease onset. *Hum Mol Genet* 18, 3039–47 (2009). [PubMed: 19465745]
- Bettencourt C et al. DNA repair pathways underlie a common genetic mechanism modulating onset in polyglutamine diseases. *Ann Neurol* 79, 983–90 (2016). [PubMed: 27044000]
- Genetic Modifiers of Huntington's Disease Consortium. Identification of genetic factors that modify clinical onset of Huntington's disease. *Cell* 162, 516–26 (2015). [PubMed: 26232222]
- Hensman Moss DJ et al. Identification of genetic variants associated with Huntington's disease progression: a genome-wide association study. *Lancet Neurol* 16, 701–711 (2017). [PubMed: 28642124]
- Gusella JF & MacDonald ME Molecular genetics: unmasking polyglutamine triggers in neurodegenerative disease. *Nat Rev Neurosci* 1, 109–15 (2000). [PubMed: 11252773]
- Rosenblatt A et al. Age, CAG repeat length, and clinical progression in Huntington's disease. *Mov Disord* 27, 272–6 (2012). [PubMed: 22173986]
- Axford MM et al. Detection of slipped-DNAs at the trinucleotide repeats of the myotonic dystrophy type I disease locus in patient tissues. *PLoS Genet* 9, e1003866 (2013). [PubMed: 24367268]
- Goula AV et al. Stoichiometry of base excision repair proteins correlates with increased somatic CAG instability in striatum over cerebellum in Huntington's disease transgenic mice. *PLoS Genet* 5, e1000749 (2009). [PubMed: 19997493]
- Lin Y, Dent SY, Wilson JH, Wells RD & Napierala M R loops stimulate genetic instability of CTG.CAG repeats. *Proc Natl Acad Sci U S A* 107, 692–7 (2010). [PubMed: 20080737]
- Pearson CE et al. Slipped-strand DNAs formed by long (CAG)*(CTG) repeats: slipped-out repeats and slip-out junctions. *Nucleic Acids Res* 30, 4534–47 (2002). [PubMed: 12384601]

17. Reddy K et al. Processing of double-R-loops in (CAG).(CTG) and C9orf72 (GGGGCC). (GGCCCC) repeats causes instability. *Nucleic Acids Res* 42, 10473–10487 (2014). [PubMed: 25147206]
18. Schmidt MH & Pearson CE Disease-associated repeat instability and mismatch repair. *DNA Repair (Amst)* 38, 117–26 (2016). [PubMed: 26774442]
19. Tome S et al. MSH3 polymorphisms and protein levels affect CAG repeat instability in Huntington's disease mice. *PLoS Genet* 9, e1003280 (2013). [PubMed: 23468640]
20. Nakamori M, Pearson CE & Thornton CA Bidirectional transcription stimulates expansion and contraction of expanded (CTG)*(CAG) repeats. *Hum Mol Genet* 20, 580–8 (2011). [PubMed: 21088112]
21. Lin Y & Wilson JH Nucleotide excision repair, mismatch repair, and R-loops modulate convergent transcription-induced cell death and repeat instability. *PLoS One* 7, e46807 (2012). [PubMed: 23056461]
22. Panigrahi GB, Slean MM, Simard JP, Gileadi O & Pearson CE Isolated short CTG/CAG DNA slip-outs are repaired efficiently by hMutSbeta, but clustered slip-outs are poorly repaired. *Proc Natl Acad Sci U S A* 107, 12593–8 (2010). [PubMed: 20571119]
23. Hagihara M & Nakatani K Inhibition of DNA replication by a d(CAG) repeat binding ligand. *Nucleic Acids Symp Ser (Oxf)*, 147–8 (2006).
24. Hagihara M, He H & Nakatani K Small molecule modulates hairpin structures in CAG trinucleotide repeats. *Chembiochem* 12, 1686–9 (2011). [PubMed: 21695756]
25. Nakatani K et al. Small-molecule ligand induces nucleotide flipping in (CAG)_n trinucleotide repeats. *Nat Chem Biol* 1, 39–43 (2005). [PubMed: 16407992]
26. Nielsen PE, Zhen WP, Henriksen U & Buchardt O Sequence-influenced interactions of oligoacridines with DNA detected by retarded gel electrophoretic migrations. *Biochemistry* 27, 67–73 (1988). [PubMed: 2831963]
27. Pluciennik A et al. Extrahelical (CAG)/(CTG) triplet repeat elements support proliferating cell nuclear antigen loading and MutLalpha endonuclease activation. *Proc Natl Acad Sci U S A* 110, 12277–82 (2013). [PubMed: 23840062]
28. Shelbourne PF et al. Triplet repeat mutation length gains correlate with cell-type specific vulnerability in Huntington disease brain. *Hum Mol Genet* 16, 1133–42 (2007). [PubMed: 17409200]
29. Silveira I et al. Trinucleotide repeats in 202 families with ataxia: a small expanded (CAG)_n allele at the SCA17 locus. *Arch Neurol* 59, 623–9 (2002). [PubMed: 11939898]
30. Sanchez-Contreras M & Cardozo-Pelaez F Age-related length variability of polymorphic CAG repeats. *DNA Repair (Amst)* 49, 26–32 (2017). [PubMed: 27865706]
31. Gao R et al. Instability of expanded CAG/CAA repeats in spinocerebellar ataxia type 17. *Eur J Hum Genet* 16, 215–22 (2008). [PubMed: 18043721]
32. Gallon R et al. A sensitive and scalable microsatellite instability assay to diagnose constitutional mismatch repair deficiency by sequencing of peripheral blood leukocytes. *Hum Mutat* 40, 649–655 (2019). [PubMed: 30740824]
33. Keohavong P, Xi L & Grant SG Molecular analysis of mutations in the human HPRT gene. *Methods Mol Biol* 291, 161–70 (2005). [PubMed: 15502221]
34. Keohavong P, Xi L & Grant SG Molecular analysis of mutations in the human HPRT gene. *Methods Mol Biol* 1105, 291–301 (2014). [PubMed: 24623237]
35. Albertini RJ et al. Mutagenicity monitoring following battlefield exposures: Longitudinal study of HPRT mutations in Gulf War I veterans exposed to depleted uranium. *Environ Mol Mutagen* 56, 581–93 (2015). [PubMed: 25914368]
36. Nicklas JA et al. Mutagenicity monitoring following battlefield exposures: Molecular analysis of HPRT mutations in Gulf War I veterans exposed to depleted uranium. *Environ Mol Mutagen* 56, 594–608 (2015). [PubMed: 25914382]
37. Poon SL, McPherson JR, Tan P, Teh BT & Rozen SG Mutation signatures of carcinogen exposure: genome-wide detection and new opportunities for cancer prevention. *Genome Med* 6, 24 (2014). [PubMed: 25031618]

38. Behjati S et al. Mutational signatures of ionizing radiation in second malignancies. *Nat Commun* 7, 12605 (2016). [PubMed: 27615322]
39. Phillips DH Mutational spectra and mutational signatures: Insights into cancer aetiology and mechanisms of DNA damage and repair. *DNA Repair (Amst)* 71, 6–11 (2018). [PubMed: 30236628]
40. Alexandrov LB et al. The repertoire of mutational signatures in human cancer. *bioRxiv* 322859; doi: 10.1101/322859.
41. Kucab JE et al. A compendium of mutational signatures of environmental agents. *Cell* 177, 821–836 e16 (2019). [PubMed: 30982602]
42. Behjati S et al. Genome sequencing of normal cells reveals developmental lineages and mutational processes. *Nature* 513, 422–425 (2014). [PubMed: 25043003]
43. Rouhani FJ et al. Mutational history of a human cell lineage from somatic to induced pluripotent stem cells. *PLoS Genet* 12, e1005932 (2016). [PubMed: 27054363]
44. Shlien A et al. Combined hereditary and somatic mutations of replication error repair genes result in rapid onset of ultra-hypermutated cancers. *Nat Genet* 47, 257–62 (2015). [PubMed: 25642631]
45. Chalmers ZR et al. Analysis of 100,000 human cancer genomes reveals the landscape of tumor mutational burden. *Genome Med* 9, 34 (2017). [PubMed: 28420421]
46. Campbell BB et al. Comprehensive analysis of hypermutation in human cancer. *Cell* 171, 1042–1056 e10 (2017). [PubMed: 29056344]
47. Hodel KP et al. Explosive mutation accumulation triggered by heterozygous human Pol epsilon proofreading-deficiency is driven by suppression of mismatch repair. *Elife* 7, e32692 (2018). [PubMed: 29488881]
48. Rayner E et al. A panoply of errors: polymerase proofreading domain mutations in cancer. *Nat Rev Cancer* 16, 71–81 (2016). [PubMed: 26822575]
49. Nakamori M, Gourdon G & Thornton CA Stabilization of expanded (CTG)*(CAG) repeats by antisense oligonucleotides. *Mol Ther* 19, 2222–7 (2011). [PubMed: 21971425]
50. Su XA & Freudenreich CH Cytosine deamination and base excision repair cause R-loop-induced CAG repeat fragility and instability in *Saccharomyces cerevisiae*. *Proc Natl Acad Sci U S A* 114, E8392–E8401 (2017). [PubMed: 28923949]
51. Lin Y, Hubert L Jr. & Wilson JH Transcription destabilizes triplet repeats. *Mol Carcinog* 48, 350–61 (2009). [PubMed: 18973172]
52. Tomé S et al. MSH2 ATPase domain mutation affects CTG*CAG repeat instability in transgenic mice. *PLoS Genet* 5, e1000482 (2009). [PubMed: 19436705]
53. McMurray CT Hijacking of the mismatch repair system to cause CAG expansion and cell death in neurodegenerative disease. *DNA Repair (Amst)* 7, 1121–34 (2008). [PubMed: 18472310]
54. Morales F et al. A polymorphism in the MSH3 mismatch repair gene is associated with the levels of somatic instability of the expanded CTG repeat in the blood DNA of myotonic dystrophy type 1 patients. *DNA Repair (Amst)* 40, 57–66 (2016). [PubMed: 26994442]
55. Flower M, et al. MSH3 modifies somatic instability and disease severity in Huntington's and myotonic dystrophy type 1. *Brain*, pii: awz115 (2019) [PubMed: 31216018]
56. Panigrahi GB, Lau R, Montgomery SE, Leonard MR & Pearson CE Slipped (CTG)*(CAG) repeats can be correctly repaired, escape repair or undergo error-prone repair. *Nat Struct Mol Biol* 12, 654–62 (2005). [PubMed: 16025129]
57. Zhang T, Huang J, Gu L & Li GM In vitro repair of DNA hairpins containing various numbers of CAG/CTG trinucleotide repeats. *DNA Repair (Amst)* 11, 201–9 (2012). [PubMed: 22041023]
58. Lai Y et al. Crosstalk between MSH2-MSH3 and polbeta promotes trinucleotide repeat expansion during base excision repair. *Nat Commun* 7, 12465 (2016). [PubMed: 27546332]
59. Tian L et al. Mismatch recognition protein MutSbeta does not hijack (CAG)_n hairpin repair in vitro. *J Biol Chem* 284, 20452–6 (2009). [PubMed: 19525234]
60. Nakatani R, Nakamori M, Fujimura H, Mochizuki H & Takahashi MP Large expansion of CTG*CAG repeats is exacerbated by MutSbeta in human cells. *Sci Rep* 5, 11020 (2015). [PubMed: 26047474]

61. Chen H, Lisby M & Symington LS RPA coordinates DNA end resection and prevents formation of DNA hairpins. *Mol Cell* 50, 589–600 (2013). [PubMed: 23706822]
62. Nguyen B et al. Diffusion of human replication protein A along single-stranded DNA. *J Mol Biol* 426, 3246–61 (2014). [PubMed: 25058683]
63. Tsurimoto T & Stillman B Multiple replication factors augment DNA synthesis by the two eukaryotic DNA polymerases, alpha and delta. *EMBO J* 8, 3883–9 (1989). [PubMed: 2573521]
64. Tsurimoto T & Stillman B Replication factors required for SV40 DNA replication in vitro. I. DNA structure-specific recognition of a primer-template junction by eukaryotic DNA polymerases and their accessory proteins. *J Biol Chem* 266, 1950–60 (1991). [PubMed: 1671045]
65. Chan NL et al. The Werner syndrome protein promotes CAG/CTG repeat stability by resolving large (CAG)(n)/(CTG)(n) hairpins. *J Biol Chem* 287, 30151–6 (2012). [PubMed: 22787159]
66. Callahan JL, Andrews KJ, Zakian VA & Freudenreich CH Mutations in yeast replication proteins that increase CAG/CTG expansions also increase repeat fragility. *Mol Cell Biol* 23, 7849–60 (2003). [PubMed: 14560028]
67. Raji NS, Krishna TH & Rao KS DNA-polymerase alpha, beta, delta and epsilon activities in isolated neuronal and astroglial cell fractions from developing and aging rat cerebral cortex. *Int J Dev Neurosci* 20, 491–6 (2002). [PubMed: 12392752]
68. Kovalenko M et al. Msh2 acts in medium-spiny striatal neurons as an enhancer of CAG instability and mutant huntingtin phenotypes in Huntington's disease knock-in mice. *PLoS One* 7, e44273 (2012). [PubMed: 22970194]
69. Mangiarini L et al. Instability of highly expanded CAG repeats in mice transgenic for the Huntington's disease mutation. *Nat Genet* 15, 197–200 (1997). [PubMed: 9020849]
70. Chiang C et al. Complex reorganization and predominant non-homologous repair following chromosomal breakage in karyotypically balanced germline rearrangements and transgenic integration. *Nat Genet* 44, 390–7, S1 (2012). [PubMed: 22388000]
71. Larson E, Fyfe I, Morton AJ & Monckton DG Age-, tissue- and length-dependent bidirectional somatic CAG*CTG repeat instability in an allelic series of R6/2 Huntington disease mice. *Neurobiol Dis* 76, 98–111 (2015). [PubMed: 25662336]
72. Kennedy L & Shelbourne PF Dramatic mutation instability in HD mouse striatum: does polyglutamine load contribute to cell-specific vulnerability in Huntington's disease? *Hum Mol Genet* 9, 2539–44 (2000). [PubMed: 11030759]
73. Ishiguro H et al. Age-dependent and tissue-specific CAG repeat instability occurs in mouse knock-in for a mutant Huntington's disease gene. *J Neurosci Res* 65, 289–97 (2001). [PubMed: 11494364]
74. Gonitell R et al. DNA instability in postmitotic neurons. *Proc Natl Acad Sci U S A* 105, 3467–72 (2008). [PubMed: 18299573]
75. De Rooij KE, De Koning Gans PA, Roos RA, Van Ommen GJ & Den Dunnen JT Somatic expansion of the (CAG)_n repeat in Huntington disease brains. *Hum Genet* 95, 270–4 (1995). [PubMed: 7868117]
76. Lee JM, Pinto RM, Gillis T, St Claire JC & Wheeler VC Quantification of age-dependent somatic CAG repeat instability in Hdh CAG knock-in mice reveals different expansion dynamics in striatum and liver. *PLoS One* 6, e23647 (2011). [PubMed: 21897851]
77. Lee JM et al. A novel approach to investigate tissue-specific trinucleotide repeat instability. *BMC Syst Biol* 4, 29 (2010). [PubMed: 20302627]
78. Wheeler VC et al. Factors associated with HD CAG repeat instability in Huntington disease. *J Med Genet* 44, 695–701 (2007). [PubMed: 17660463]
79. Higham CF, Morales F, Cobbold CA, Haydon DT & Monckton DG High levels of somatic DNA diversity at the myotonic dystrophy type 1 locus are driven by ultra-frequent expansion and contraction mutations. *Hum Mol Genet* 21, 2450–63 (2012). [PubMed: 22367968]
80. Veitch NJ et al. Inherited CAG/CTG allele length is a major modifier of somatic mutation length variability in Huntington disease. *DNA Repair (Amst)* 6, 789–96 (2007). [PubMed: 17293170]
81. Hornsby PJ & Didenko VV In situ ligation: a decade and a half of experience. *Methods Mol Biol* 682, 49–63 (2011). [PubMed: 21057920]

82. Majtnerova P & Rousar T An overview of apoptosis assays detecting DNA fragmentation. *Mol Biol Rep* 45, 1469–1478 (2018). [PubMed: 30022463]
83. Iannicola C et al. Early alterations in gene expression and cell morphology in a mouse model of Huntington's disease. *J Neurochem* 75, 830–9 (2000). [PubMed: 10899961]
84. Turmaine M et al. Nonapoptotic neurodegeneration in a transgenic mouse model of Huntington's disease. *Proc Natl Acad Sci U S A* 97, 8093–7 (2000). [PubMed: 10869421]
85. Yu ZX et al. Mutant huntingtin causes context-dependent neurodegeneration in mice with Huntington's disease. *J Neurosci* 23, 2193–202 (2003). [PubMed: 12657678]
86. DiFiglia M et al. Aggregation of huntingtin in neuronal intranuclear inclusions and dystrophic neurites in brain. *Science* 277, 1990–3 (1997). [PubMed: 9302293]
87. Li SH & Li XJ Aggregation of N-terminal huntingtin is dependent on the length of its glutamine repeats. *Hum Mol Genet* 7, 777–82 (1998). [PubMed: 9536080]
88. Becher MW et al. Intranuclear neuronal inclusions in Huntington's disease and dentatorubral and pallidolusian atrophy: correlation between the density of inclusions and IT15 CAG triplet repeat length. *Neurobiol Dis* 4, 387–97 (1998). [PubMed: 9666478]
89. Li H et al. Ultrastructural localization and progressive formation of neuropil aggregates in Huntington's disease transgenic mice. *Hum Mol Genet* 8, 1227–36 (1999). [PubMed: 10369868]
90. Li H, Li SH, Johnston H, Shelbourne PF & Li XJ Amino-terminal fragments of mutant huntingtin show selective accumulation in striatal neurons and synaptic toxicity. *Nat Genet* 25, 385–9 (2000). [PubMed: 10932179]
91. Carty N et al. Characterization of HTT inclusion size, location, and timing in the zQ175 mouse model of Huntington's disease: an in vivo high-content imaging study. *PLoS One* 10, e0123527 (2015). [PubMed: 25859666]
92. Kaytor MD, Wilkinson KD & Warren ST Modulating huntingtin half-life alters polyglutamine-dependent aggregate formation and cell toxicity. *J Neurochem* 89, 962–73 (2004). [PubMed: 15140195]
93. Coufal M et al. Discovery of a novel small-molecule targeting selective clearance of mutant huntingtin fragments. *J Biomol Screen* 12, 351–60 (2007). [PubMed: 17379859]
94. Chopra V et al. A small-molecule therapeutic lead for Huntington's disease: preclinical pharmacology and efficacy of C2–8 in the R6/2 transgenic mouse. *Proc Natl Acad Sci U S A* 104, 16685–9 (2007). [PubMed: 17925440]
95. Butler DC & Messer A Bifunctional anti-huntingtin proteasome-directed intrabodies mediate efficient degradation of mutant huntingtin exon 1 protein fragments. *PLoS One* 6, e29199 (2011). [PubMed: 22216210]
96. Perucho J et al. Striatal infusion of glial conditioned medium diminishes huntingtin pathology in r6/1 mice. *PLoS One* 8, e73120 (2013). [PubMed: 24069174]
97. Tsvetkov AS et al. Proteostasis of polyglutamine varies among neurons and predicts neurodegeneration. *Nat Chem Biol* 9, 586–92 (2013). [PubMed: 23873212]
98. Penney JB Jr., Vonsattel JP, MacDonald ME, Gusella JF & Myers RH CAG repeat number governs the development rate of pathology in Huntington's disease. *Ann Neurol* 41, 689–92 (1997). [PubMed: 9153534]
99. Wheeler VC et al. Long glutamine tracts cause nuclear localization of a novel form of huntingtin in medium spiny striatal neurons in HdhQ92 and HdhQ111 knock-in mice. *Hum Mol Genet* 9, 503–13 (2000). [PubMed: 10699173]
100. Rosenblatt A et al. Does CAG repeat number predict the rate of pathological changes in Huntington's disease? *Ann Neurol* 44, 708–9 (1998). [PubMed: 9778276]
101. Wild EJ & Tabrizi SJ Therapies targeting DNA and RNA in Huntington's disease. *Lancet Neurol* 16, 837–847 (2017). [PubMed: 28920889]
102. Dabrowska M, Juzwa W, Krzyzosiak WJ & Olejniczak M Precise Excision of the CAG Tract from the Huntingtin Gene by Cas9 Nickases. *Front Neurosci* 12, 75 (2018). [PubMed: 29535594]
103. Shin JW et al. Permanent inactivation of Huntington's disease mutation by personalized allele-specific CRISPR/Cas9. *Hum Mol Genet* 25, 4566–4576 (2016). [PubMed: 28172889]

104. Monteys AM, Ebanks SA, Keiser MS & Davidson BL CRISPR/Cas9 Editing of the Mutant Huntingtin Allele In Vitro and In Vivo. *Mol Ther* 25, 12–23 (2017). [PubMed: 28129107]
105. Cinesi C, Aeschbach L, Yang B & Dion V Contracting CAG/CTG repeats using the CRISPR-Cas9 nickase. *Nat Commun* 7, 13272 (2016). [PubMed: 27827362]
106. Suelves N, Kirkham-McCarthy L, Lahue RS & Gines S A selective inhibitor of histone deacetylase 3 prevents cognitive deficits and suppresses striatal CAG repeat expansions in Huntington's disease mice. *Sci Rep* 7, 6082 (2017). [PubMed: 28729730]
107. Eisenstein M CRISPR takes on Huntington's disease. *Nature* 557, S42–S43 (2018). [PubMed: 29844549]
108. Martins S et al. Modifiers of (CAG)(n) instability in Machado-Joseph disease (MJD/SCA3) transmissions: an association study with DNA replication, repair and recombination genes. *Hum Genet* 133, 1311–8 (2014). [PubMed: 25026993]
109. Moss DJH et al. Identification of genetic variants associated with Huntington's disease progression: a genome-wide association study. *Lancet Neurol* 16, 701–711 (2017). [PubMed: 28642124]
110. Guo J, Gu L, Leffak M & Li GM MutSbeta promotes trinucleotide repeat expansion by recruiting DNA polymerase beta to nascent (CAG)n or (CTG)n hairpins for error-prone DNA synthesis. *Cell Res* 26, 775–86 (2016). [PubMed: 27255792]
111. Hanawalt PC & Spivak G Transcription-coupled DNA repair: two decades of progress and surprises. *Nat Rev Mol Cell Biol* 9, 958–70 (2008). [PubMed: 19023283]
112. Hou C, Chan NL, Gu L & Li GM Incision-dependent and error-free repair of (CAG)(n)/(CTG)(n) hairpins in human cell extracts. *Nat Struct Mol Biol* 16, 869–75 (2009). [PubMed: 19597480]
113. Chan NL et al. Coordinated processing of 3' slipped (CAG)n/(CTG)n hairpins by DNA polymerases beta and delta preferentially induces repeat expansions. *J Biol Chem* 288, 15015–22 (2013). [PubMed: 23585564]
114. Pinto RM et al. Mismatch repair genes Mlh1 and Mlh3 modify CAG instability in Huntington's disease mice: genome-wide and candidate approaches. *PLoS Genet* 9, e1003930 (2013). [PubMed: 24204323]
115. Wheeler VC et al. Mismatch repair gene Msh2 modifies the timing of early disease in Hdh(Q111) striatum. *Hum Mol Genet* 12, 273–81 (2003). [PubMed: 12554681]
116. Strobel SA, Doucette-Stamm LA, Riba L, Housman DE & Dervan PB Site-specific cleavage of human chromosome 4 mediated by triple-helix formation. *Science* 254, 1639–42 (1991). [PubMed: 1836279]
117. Mittelman D et al. Zinc-finger directed double-strand breaks within CAG repeat tracts promote repeat instability in human cells. *Proc Natl Acad Sci U S A* 106, 9607–12 (2009). [PubMed: 19482946]
118. Zeitler B et al. Allele-selective transcriptional repression of mutant HTT for the treatment of Huntington's disease. *Nat Med* 25, 1131–1142 (2019). [PubMed: 31263285]
119. Mosbach V, Poggi L & Richard GF Trinucleotide repeat instability during double-strand break repair: from mechanisms to gene therapy. *Curr Genet* 65, 17–28 (2019). [PubMed: 29974202]
120. Malankhanova TB, Malakhova AA, Medvedev SP & Zakian SM Modern genome editing technologies in Huntington's disease research. *J Huntingtons Dis* 6, 19–31 (2017). [PubMed: 28128770]
121. Babacic H, Mehta A, Merkel O & Schoser B CRISPR-cas gene-editing as plausible treatment of neuromuscular and nucleotide-repeat-expansion diseases: A systematic review. *PLoS One* 14, e0212198 (2019). [PubMed: 30794581]
122. Gomes-Pereira M & Monckton DG Chemical modifiers of unstable expanded simple sequence repeats: what goes up, could come down. *Mutat Res* 598, 15–34 (2006). [PubMed: 16500684]
123. Pineiro E et al. Mutagenic stress modulates the dynamics of CTG repeat instability associated with myotonic dystrophy type 1. *Nucleic Acids Res* 31, 6733–40 (2003). [PubMed: 14627806]
124. Budworth H et al. Suppression of somatic expansion delays the onset of pathophysiology in a mouse model of Huntington's disease. *PLoS Genet* 11, e1005267 (2015). [PubMed: 26247199]
125. Gottesfeld JM, Neely L, Trauger JW, Baird EE & Dervan PB Regulation of gene expression by small molecules. *Nature* 387, 202–5 (1997). [PubMed: 9144294]

126. Leontieva OV & Blagosklonny MV CDK4/6-inhibiting drug substitutes for p21 and p16 in senescence: duration of cell cycle arrest and MTOR activity determine geroconversion. *Cell Cycle* 12, 3063–9 (2013). [PubMed: 23974099]
127. Nakamori M, Sobczak K, Moxley RT & Thornton CA Scaled-down genetic analysis of myotonic dystrophy type 1 and type 2. *Neuromuscul Disord* 19, 759–62 (2009). [PubMed: 19713112]
128. Brook JD et al. Molecular basis of myotonic dystrophy: expansion of a trinucleotide (CTG) repeat at the 3' end of a transcript encoding a protein kinase family member. *Cell* 69, 385 (1992).
129. Dietmaier W et al. Diagnostic microsatellite instability: definition and correlation with mismatch repair protein expression. *Cancer Res* 57, 4749–56 (1997). [PubMed: 9354436]
130. Kabbarah O et al. A panel of repeat markers for detection of microsatellite instability in murine tumors. *Mol Carcinog* 38, 155–9 (2003). [PubMed: 14639654]
131. Koob MD et al. An untranslated CTG expansion causes a novel form of spinocerebellar ataxia (SCA8). *Nat Genet* 21, 379–84 (1999). [PubMed: 10192387]
132. Kremer B et al. Sex-dependent mechanisms for expansions and contractions of the CAG repeat on affected Huntington disease chromosomes. *Am J Hum Genet* 57, 343–50 (1995). [PubMed: 7668260]
133. Cleary JD, Nichol K, Wang YH & Pearson CE Evidence of cis-acting factors in replication-mediated trinucleotide repeat instability in primate cells. *Nat Genet* 31, 37–46 (2002). [PubMed: 11967533]
134. Panigrahi GB, Cleary JD & Pearson CE In vitro (CTG)ⁿ(CAG) expansions and deletions by human cell extracts. *J Biol Chem* 277, 13926–34 (2002). [PubMed: 11832482]
135. Reddy K et al. Determinants of R-loop formation at convergent bidirectionally transcribed trinucleotide repeats. *Nucleic Acids Res* 39, 1749–62 (2011). [PubMed: 21051337]
136. Binz SK, Dickson AM, Haring SJ & Wold MS Functional assays for replication protein A (RPA). *Methods Enzymol* 409, 11–38 (2006). [PubMed: 16793393]
137. Zhou Y, Meng X, Zhang S, Lee EY & Lee MY Characterization of human DNA polymerase delta and its subassemblies reconstituted by expression in the MultiBac system. *PLoS One* 7, e39156 (2012). [PubMed: 22723953]
138. Mason AC, Roy R, Simmons DT & Wold MS Functions of alternative replication protein A in initiation and elongation. *Biochemistry* 49, 5919–28 (2010). [PubMed: 20545304]
139. Tome S et al. Tissue-specific mismatch repair protein expression: MSH3 is higher than MSH6 in multiple mouse tissues. *DNA Repair (Amst)* 12, 46–52 (2013). [PubMed: 23228367]
140. Jeon I et al. Human-to-mouse prion-like propagation of mutant huntingtin protein. *Acta Neuropathol* 132, 577–92 (2016). [PubMed: 27221146]
141. Cibulskis K et al. Sensitive detection of somatic point mutations in impure and heterogeneous cancer samples. *Nat Biotechnol* 31, 213–9 (2013). [PubMed: 23396013]
142. Morgulis A, Gertz EM, Schaffer AA & Agarwala R A fast and symmetric DUST implementation to mask low-complexity DNA sequences. *J Comput Biol* 13, 1028–40 (2006). [PubMed: 16796549]
143. Li H Toward better understanding of artifacts in variant calling from high-coverage samples. *Bioinformatics* 30, 2843–51 (2014). [PubMed: 24974202]
144. Alexandrov LB et al. Signatures of mutational processes in human cancer. *Nature* 500, 415–21 (2013). [PubMed: 23945592]
145. Alexandrov LB, Nik-Zainal S, Wedge DC, Campbell PJ & Stratton MR Deciphering signatures of mutational processes operative in human cancer. *Cell Rep* 3, 246–59 (2013). [PubMed: 23318258]
146. Nik-Zainal S et al. Landscape of somatic mutations in 560 breast cancer whole-genome sequences. *Nature* 534, 47–54 (2016). [PubMed: 27135926]
147. Li H & Durbin R Fast and accurate long-read alignment with Burrows-Wheeler transform. *Bioinformatics* 26, 589–95 (2010). [PubMed: 20080505]

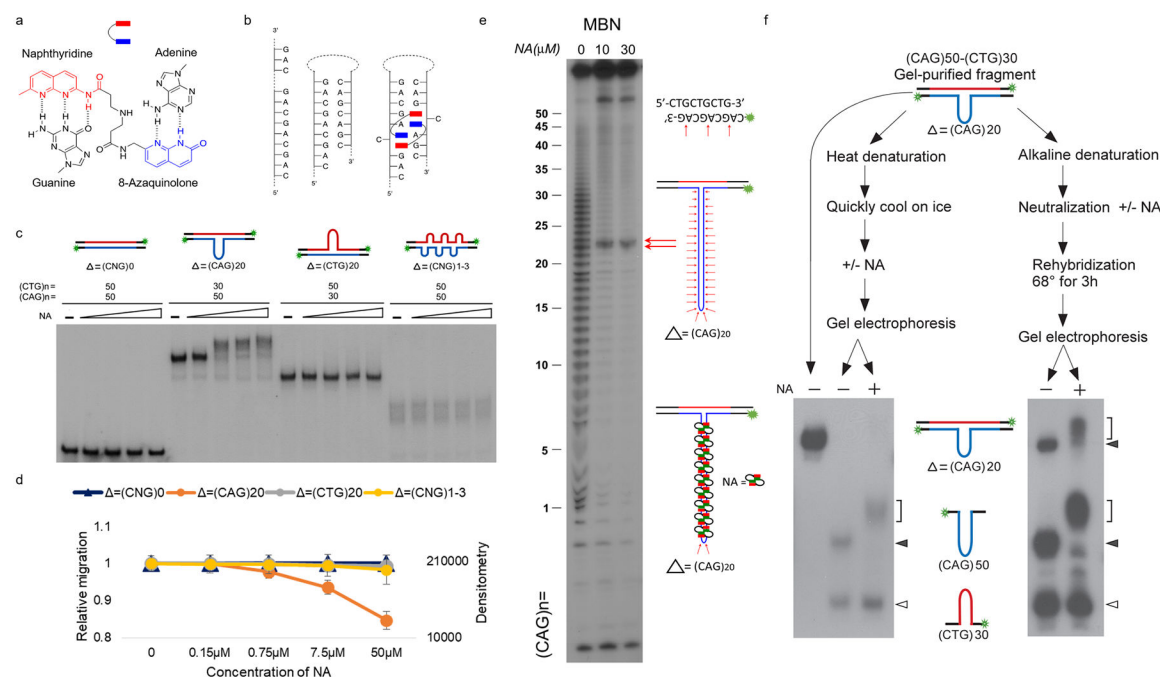


Figure 1 | NA binds to long CAG slip-outs.

a, Structure of NA comprising two heterocycles, naphthyridine (red) and 8-azaquinolone moiety (blue)²⁵. **b**, Schematic of NA-(CAG)_n-(CAG)_n triad complex revealed by NMR spectroscopy²⁵. The (CAG)_n DNA sequence (left) can fold into hairpins involving mismatched A-A pairs flanked by C-G and G-C pairs (middle). NA molecules intercalate into the DNA helix, with the 2-amino-1,8-naphthyridine moiety hydrogen bonding to guanine (in red) and 8-azaquinolone moiety hydrogen bonding to adenine (in blue), forcing the flipped-out cytosine bases. **c**, Binding of NA to gel-purified DNA fragments with (CAG)_n•(CAG)_n repeats in both strands flanked by 59 bp and 54 bp of non-repetitive DNA labeled with ³²P-labeled on both strands (green star). **d**, Quantification of NA binding. Relative migration was measured as the ratio of migration distance of each NA-DNA complex to the migration distance of free DNA. Densitometric analysis was performed for the (CNG)1–3 DNA substrate. Graphs indicate the mean of three independent experiments +/– standard deviation (s.d.). **e**, Footprinting on (CAG)₅₀•(CTG)₃₀ uniquely ³²P-labeled on the (CAG)₅₀ strand, cleaved throughout the repeat using mung bean nuclease (MBN)¹⁶. In the presence of NA, all scissile sites (red arrows) with the exception of the hairpin tip, are protected, revealing binding specificity for the slip-out stem. Two independent experiments were performed with similar results. **f**, Gel-purified DNAs with a long (CAG)₂₀ slip-out from (CAG)₅₀•(CTG)₃₀, ³²P-labeled on both strands, were treated as indicated and resolved on 4% polyacrylamide. NA-DNA complexes formed with both the (CAG)₅₀ strand (both panels) and the heteroduplexed (CAG)₅₀•(CTG)₃₀ (right panel) are shown by brackets; free DNA is indicated by arrowheads. NA did not bind (CTG)₃₀ hairpin fragment in either experiment (white arrowheads), and did not inhibit re-hybridization of complementary strands. Two independent experiments were performed with similar results. Blots have been cropped and the corresponding full blots are available in the Source Data files.

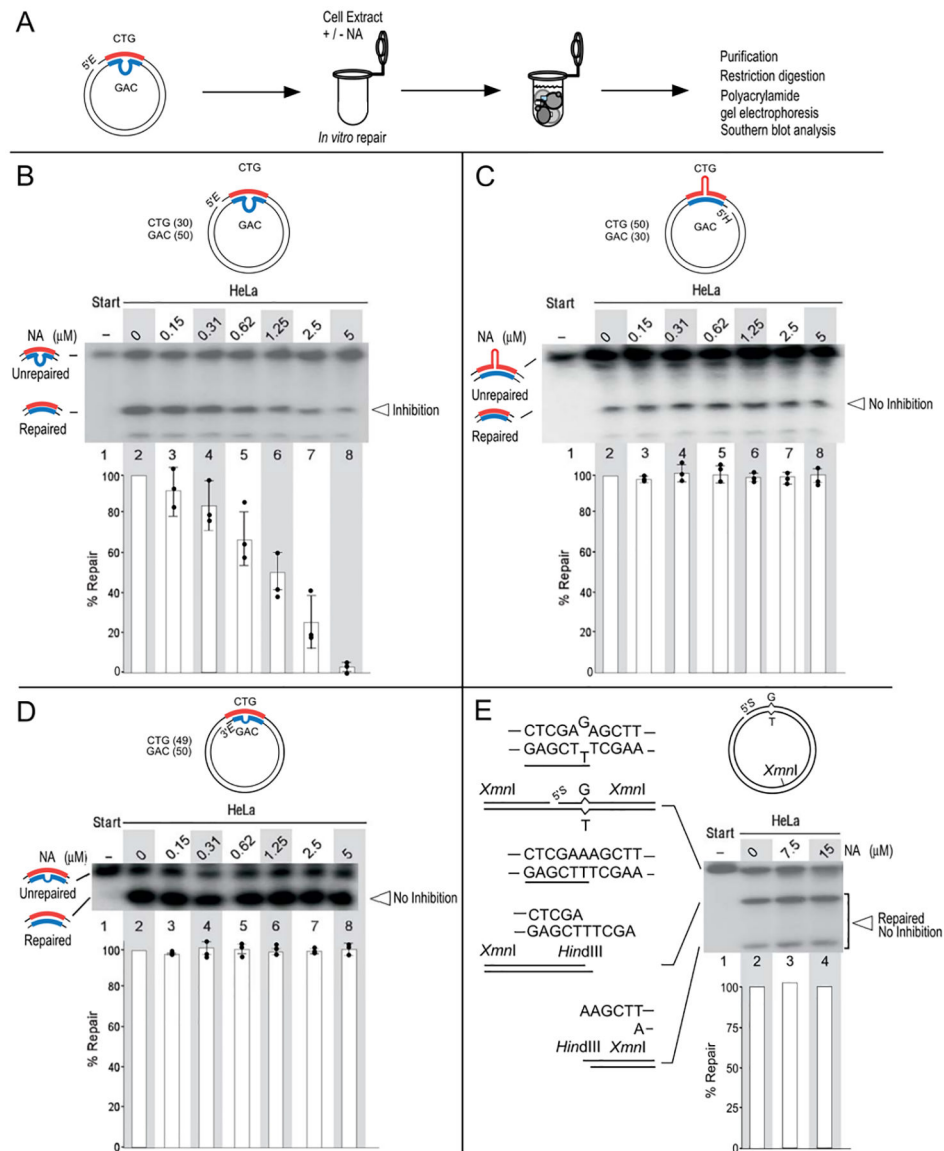


Figure 2 | NA specifically inhibits repair of long CAG slip-outs by human (HeLa) cell extracts.
a. Schematic of the *in vitro* repair assay. **b-e.** Starting DNAs and repair products (schematics) have the repeat-containing fragment released, resolved on PAGE and assessed on a molar level by Southern blotting and densitometry. Repair of DNA substrates containing a long (CAG)20 slip-out (**b**), a long (CTG)20 slip-out (**c**), a single CAG slip-out (**d**), or a G-T base-base mismatch (**e**), in the absence or presence of NA. Slipped-DNAs were hybrids of (CAG)50•(CTG)30, (CAG)30•(CTG)50 or (CAG)50•(CTG)49 (Methods)^{22,56}. Repair of the G-T mismatch reconstitutes a *HindIII* restriction site. Graphs show percentage repair efficiencies to repaired product relative to all repeat-containing fragments in the lane; values are normalized to the NA-free efficiency. Values represent the mean of three independent experiments \pm s.d. Blots have been cropped and the corresponding full blots are available in the Source Data files.

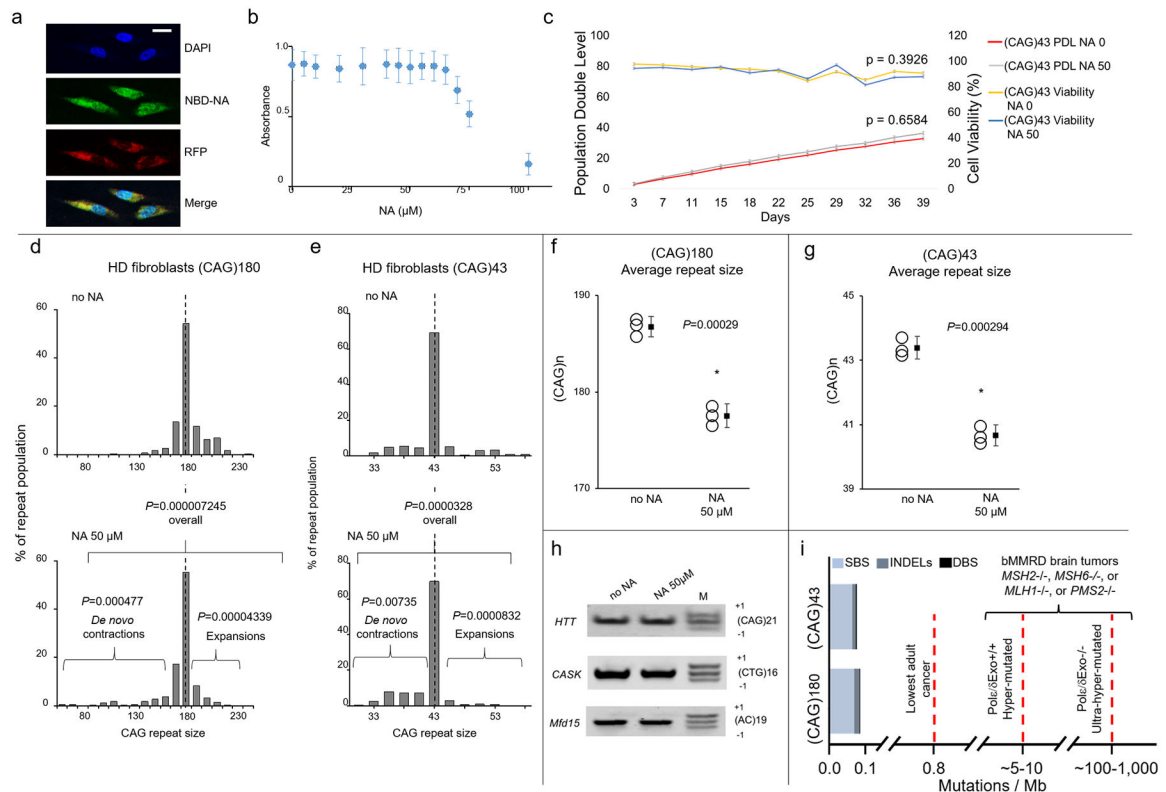


Figure 3 | NA cellular distribution, non-toxicity, and effects on repeat instability in HD patient cells.

a, NBD-labeled NA (green) was distributed throughout nuclei and cytoplasm of human HD primary fibroblasts with (CAG)43 (GM02191). Nuclei and cell membranes were stained with DAPI (blue) and Cell Light Plasma Membrane-RFP (red), respectively. Scale bar: 20 μM. Three independent experiments were performed. **b**, Cell toxicity of (CAG)43 cells treated with NA for 72 h. Viability estimated by WST-1 assays. Values represent means of three independent measures \pm s.d.. **c**, Population doubling levels and percentage of cell viability of (CAG)43 cells treated with or without 50 μM NA. Error bars indicate the s.d. of three independent experiments. Unpaired two-tailed *t*-test was used to calculate *P*-values. **d,e**, Repeat instability was analyzed by small-pool-PCR across the HD repeat tract (Methods, see Supplementary Table 1). Histograms show repeat-length distributions in human HD primary fibroblasts with (CAG)180⁵ (GM09197) or with (CAG)43 (GM02191), after 40 days growth \pm NA. Frequency distribution of repeat alleles is indicated as gray bars. Dashed line indicates peak CAG size. Allele lengths are grouped in bins spanning 10 repeats; >230 alleles were sized per group. Percentage of repeat population was calculated by dividing the number of alleles grouped in bins spanning 10 repeats by the number of total alleles. Shown is a summary of 3 independent experiments. *P*-values were calculated by χ^2 -test comparing the frequencies of expanded, unchanged, and contracted alleles in each set of experiments (Supplementary Table 1). **f,g**, Average (mean) repeat size in HD fibroblasts after 40 days incubation with or without NA. **P* < 0.001, two-sided Student's *t* test. Error bars: 99% confidence limits. **h**, Repeat lengths of the *HTT* (normal allele), *CASK*, and *Mfd15* loci in HD fibroblast cells (after 40 days incubation \pm NA). Three independent

experiments were performed. **i**, Rate of single base substitutions (SBS), insertions/deletions (INDELs), and double substitutions (DBS) in NA-treated HD cells with (CAG)43 or (CAG)180 compared to mock-treated cells. SBS/INDELs/DBS/rearrangements detected in the NA-treated (CAG)43 or (CAG)180 cells were 172/29/7/0 and 187/42/5/0, respectively. Dashed lines indicate the 0.8 mutations/Mb, which is the lowest burden observed in a typically “quiet” adult cancer (bone marrow myelodysplastic syndrome⁴⁵), and the 5–10 and 100–1,000 mutations/Mb in biallelic mismatch repair deficient cancers, with and without polExpo activity^{44–48}. Blots have been cropped and the corresponding full blots are available in the Source Data files.

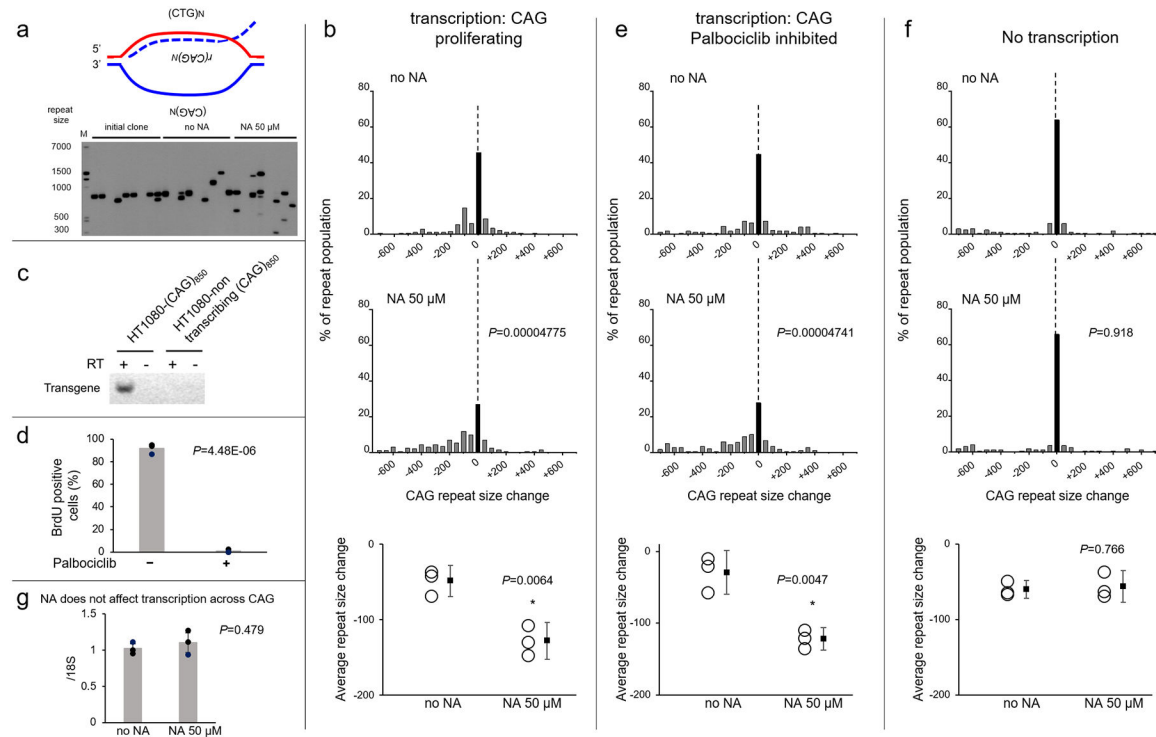


Figure 4 | NA induces CAG contractions, independent of proliferation, dependent on rCAG transcription.

a. Schematic transcription bubble, and representative data showing spPCR repeat length analysis of HT1080-(CAG)850 cells (initial cell clone and cells after 30 days incubation +/- NA) (Methods)^{20,49}. Scale at left shows molecular weight markers (M) converted into repeat number for CAG-repeat fragments of equivalent size. **b.** Histograms showing repeat length distributions, after 30 days incubation +/- NA, in proliferating HT1080-(CAG)850 cells, in which transcription was permissible. Mean repeat size change is shown below. Frequency distribution of unstable and stable alleles is shown by gray bars and black bars, respectively. Dashed lines indicates the unchanged CAG size. Allele lengths are grouped in bins spanning 50 repeats. Percentage of repeat population was calculated by dividing the number of alleles grouped in bins by the number of total alleles; >50 alleles were sized for each group (Supplementary Table 1). *P*-values were calculated by χ^2 -test. Error bars: 99% confidence limits. Shown is a summary of 3 independent experiments. **c.** RT-PCR analysis of the CAG repeat in HT1080-non-transcribing cells, showing that the transgene is integrated as a single copy. Three independent experiments were performed. **d.** BrdU-positive cells after 24 h incubation with BrdU in Palbociclib-treated HT1080-(CAG)850 cells. *P*-value was calculated by *t*-test. Data are the mean \pm s.d. of triplicates. **e.** Histograms showing repeat length distributions after 30 days incubation with or without NA, in non-proliferating (Palbociclib-arrested) HT1080-(CAG)850 cells. Mean repeat size change is shown below. *P*-values were calculated by χ^2 -test (Supplementary Table 1). Error bars: 99% confidence limits. Shown is a summary of 3 independent experiments. **f.** Histograms showing repeat length distributions after 30 days incubation with or without NA, in non-transcribing HT1080-(CAG)850 cells. Mean repeat size change is shown below. *P*-values were calculated by χ^2 -test (Supplementary Table 1). Error bars: 99% confidence limits. Shown is a summary

of 3 independent experiments. **g**, RNA transcript levels of transgene (transcript in the CAG-direction) in HT1080–(CAG)850 cells treated with or without NA (50 μ M)⁴⁹. Data are the mean \pm s.d. of triplicates; *t*-test (two-sided) was used for independent biological triplicate experiments. Blots have been cropped and the corresponding full blots are available in the Source Data files.

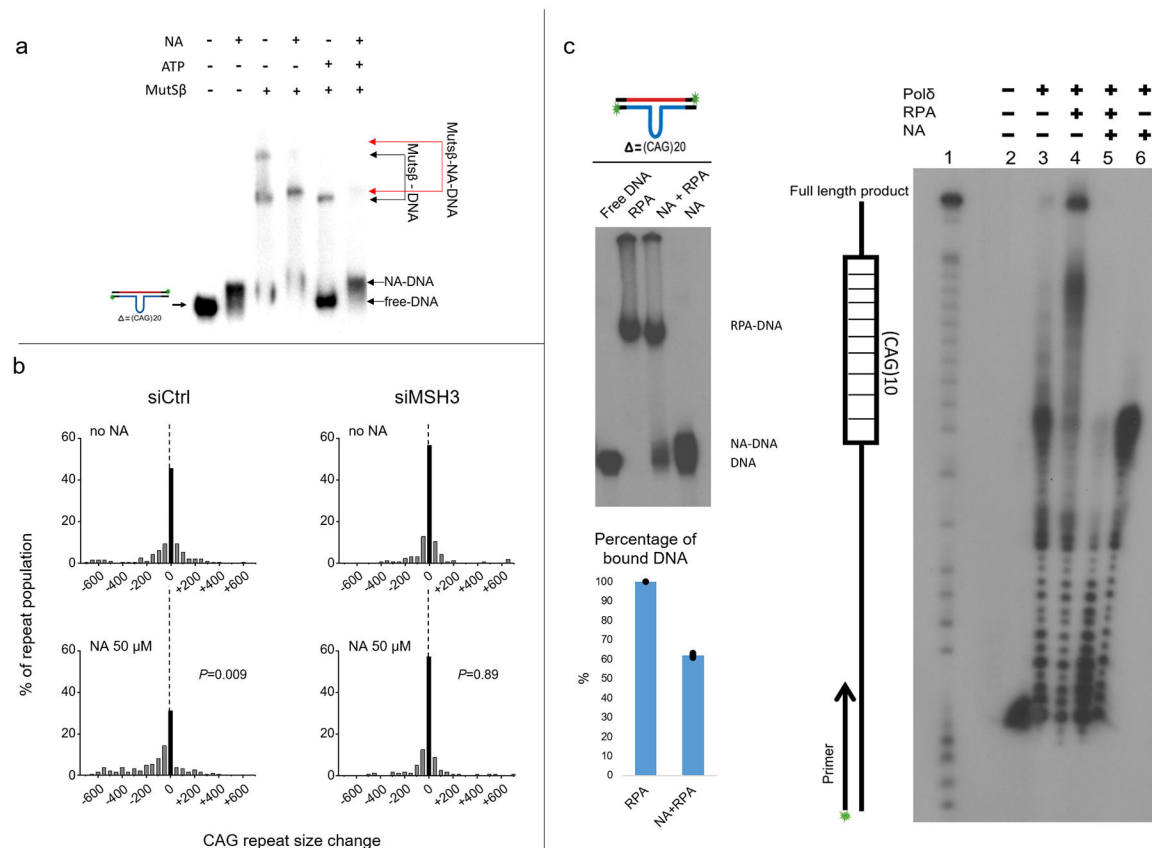


Figure 5 | NA affects interaction of DNA repair proteins on long CAG slip-outs.

a, MutS β binding to radiolabelled slipped-DNA (CAG)50•(CTG)30 containing a single (CAG)20 slip-out at room temperature for 30 min. Addition of ATP (+/- Mg²⁺) disrupts binding of MutS β to the DNA, as described⁵⁹. Addition of NA has no effect on binding or dissociation of MutS β with this substrate. **b**, Histograms showing repeat length distributions in HT1080-(CAG)850 cells treated with control siRNA (left) and siRNA against MSH3 (right), +/- NA. Frequency distribution of unstable and stable alleles is shown by gray and black bars, respectively. Dashed lines indicate unchanged CAG size. Percentage of repeat population was calculated by dividing the number of alleles grouped in bins spanning 50 repeats by the number of total alleles; >50 alleles were sized for each group (Supplementary Table 1). *P*-values were calculated by χ^2 -test. Error bars: 99% confidence limits. Shown is a summary of 3 independent experiments. **c**, RPA (250 nM) binding to slipped-DNA (CAG)50•(CTG)30 containing a single (CAG)20 slip-out (lane 2), ³²P-labeled on both strands (schematic on top). DNA was incubated with NA (50-microM) for 10 min at room temperature, prior to addition of RPA. Percentage of RPA-bound DNA quantified by densitometry. Histograms indicate mean of three independent experiments +/- s.d. **d**, Polymerase extension assay performed as described²³. (CAG)10 template oligo was annealed with a ³²P-labeled primer and incubated +/-NA (50 μ M) for 30 min at room temperature. 250 nM RPA and/or 20 nM Pol δ was added and incubated for 15 min at 37 °C. Products were separated on a 6% sequencing gel together with Maxam-Gilbert sequencing reactions (lane 1). Primer only is in lane 2. Three independent experiments were performed.

Blots have been cropped and the corresponding full blots are available in the Source Data files.

Author Manuscript

Author Manuscript

Author Manuscript

Author Manuscript

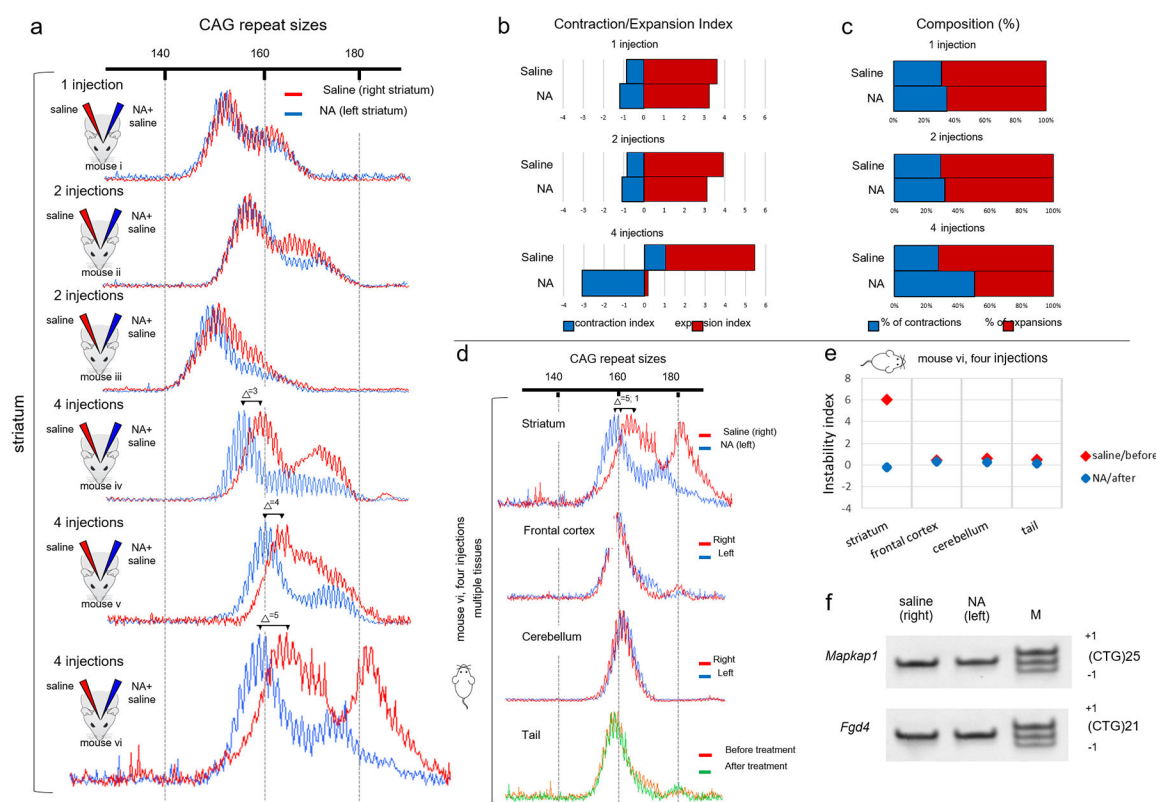


Fig. 6]. NA induces CAG contractions in R6/2 mouse striatum.

a, GeneMapper traces showing the distribution of CAG-repeat lengths in striatum from six representative 10-week-old R6/2 mice that received one (mouse 1), two (mice 2 and 3) or four (mice 4–6) injections of NA, over a 4-week period. NA, dissolved in saline, was injected into the left striatum (blue) and saline alone was injected into the right striatum (red). All mice treated four times are shown in Supplementary Figs. 3–6. **b**, The effect of one, two or four NA injections reflected by contraction and expansion instability indices (Methods)^{77,78}. **c**, The effect of one, two or four NA injections reflected by the relative composition of contractions and expansions (Methods)^{77,78}. **d**, The CAG length distributions by GeneMapper traces in the striatum, frontal cortex, cerebellum and tail from one representative R6/2 mouse (mouse 6) following four injections of NA into the left striatum, over a 4-week period. DNAs were isolated from the left (NA, blue) and right (saline, red) sides of the striatum, frontal cortex and cerebellum, and from the tail before (red) and after (green) NA treatment. The repeat size change is in brackets, with the first number representing the NA-induced contractions of the major peak relative to the somatic expansions without NA, and the second number representing the contractions relative to the inherited (tail) allele. The brackets do not account for the size changes in the second mode of the bimodal distribution in the striatum. **e**, Instability indices in various tissues shown in d, where the red and blue diamonds represent values of the saline-treated/right and NA-treated/left sides of the striatum, respectively. **f**, The repeat tract lengths of the *Mapkap1* and *Fgd4* loci in both sides of the striatum from an R6/2 mouse with four injections. Three independent experiments were performed. Uncropped gels are available as source data.

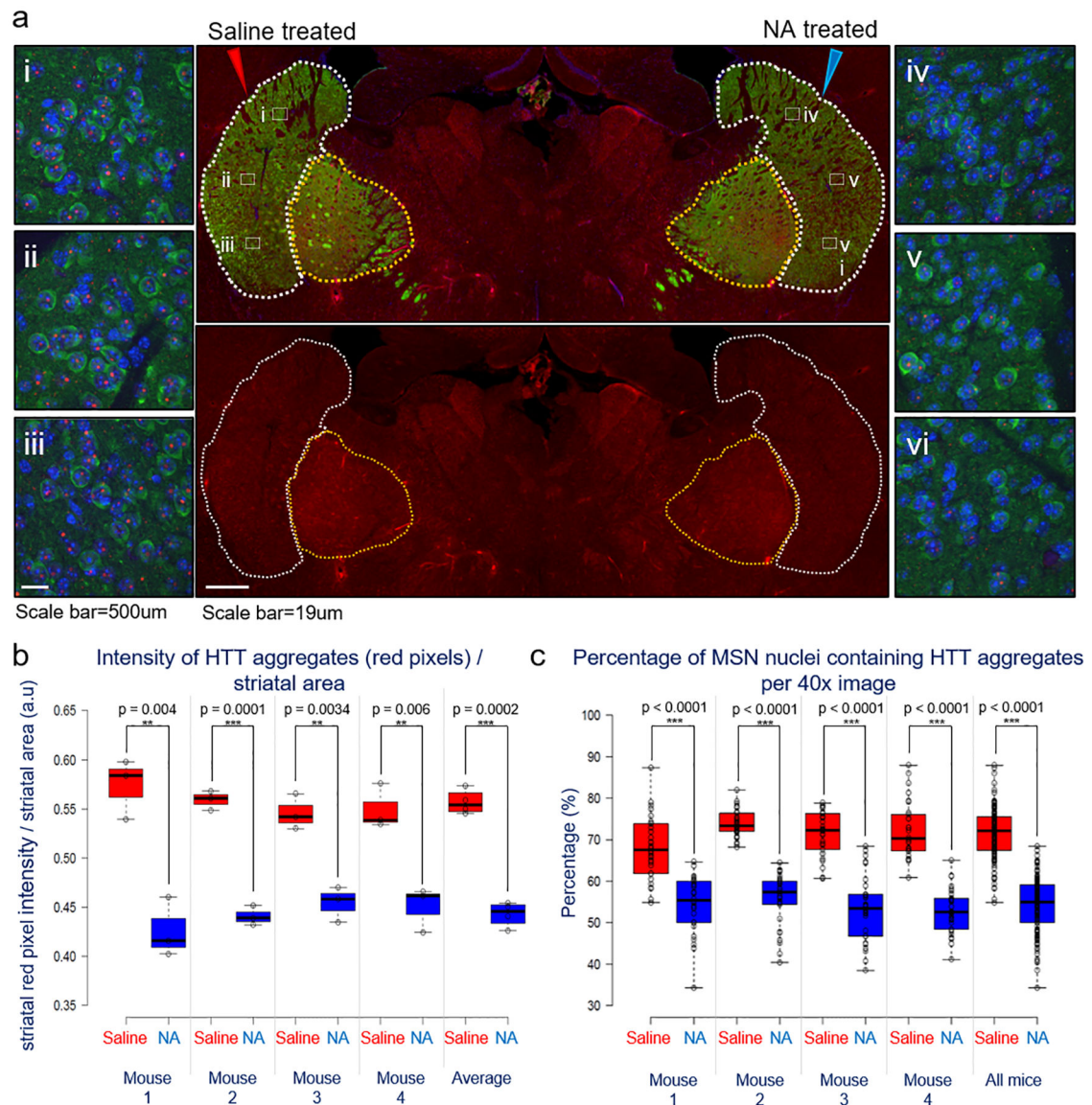


Fig. 7]. NA induces a reduction in mHTT aggregates in R6/2 mice.

The effect of NA on mHTT aggregates in striatal MSNs of R6/2 mice treated with saline (right striata) and 50 μ M NA (left striata), the slide indicates saline- and NA-treated halves with red and blue arrowheads, respectively. **a**, Top middle panel: a representative $\times 20$ magnification epifluorescent image of a whole-brain slice stained for DARPP-32 (green, staining MSNs), mHTT aggregates (red) and counterstained with DAPI (blue). The numerals and associated dotted white squares mark the location of the corresponding representative $\times 40$ magnification confocal images for saline-treated (i, ii, iii) and NA-treated (iv, v, vi) striata. The dotted lines demarcate borders of striatum (DARPP-32-positive cells) with the white dotted lines demarcating borders of striatal cell bodies (used for quantification) and the yellow dotted lines demarcating axons that form striatonigral bundles (not used for quantification). Bottom middle panel: the mHTT (red) channel alone. Scale bars, 19 μ m (magnifications) and 500 μ m (middle panels). **b**, Quantification by box plots of the red pixel

intensity per striatal area in R6/2 mouse striatum treated with saline (right striata) and 50 μ M NA (left striata) obtained via ImageJ quantification of $\times 20$ mHTT/red channel epifluorescent images (4 mice total, 3 slides quantified per mouse, 30 images per mouse, 60–75 cells per image). An unpaired two-tailed *t*-test was used to compare the intensity of the red pixels in treated versus untreated striata. **c**, Quantification of the percentage of MSN nuclei containing mHTT aggregates in R6/2 mouse striatum treated with saline (right striata) and 50 μ M NA (left striata) obtained via counting of mHTT-positive MSN nuclei in $\times 40$ confocal images (4 mice total, 3 slides quantified per mouse, 10 images quantified per striata, ~50–100 cells per image). An unpaired two-tailed *t*-test was used to compare the percentage of MSN nuclei containing mHTT aggregates in treated versus untreated striata.

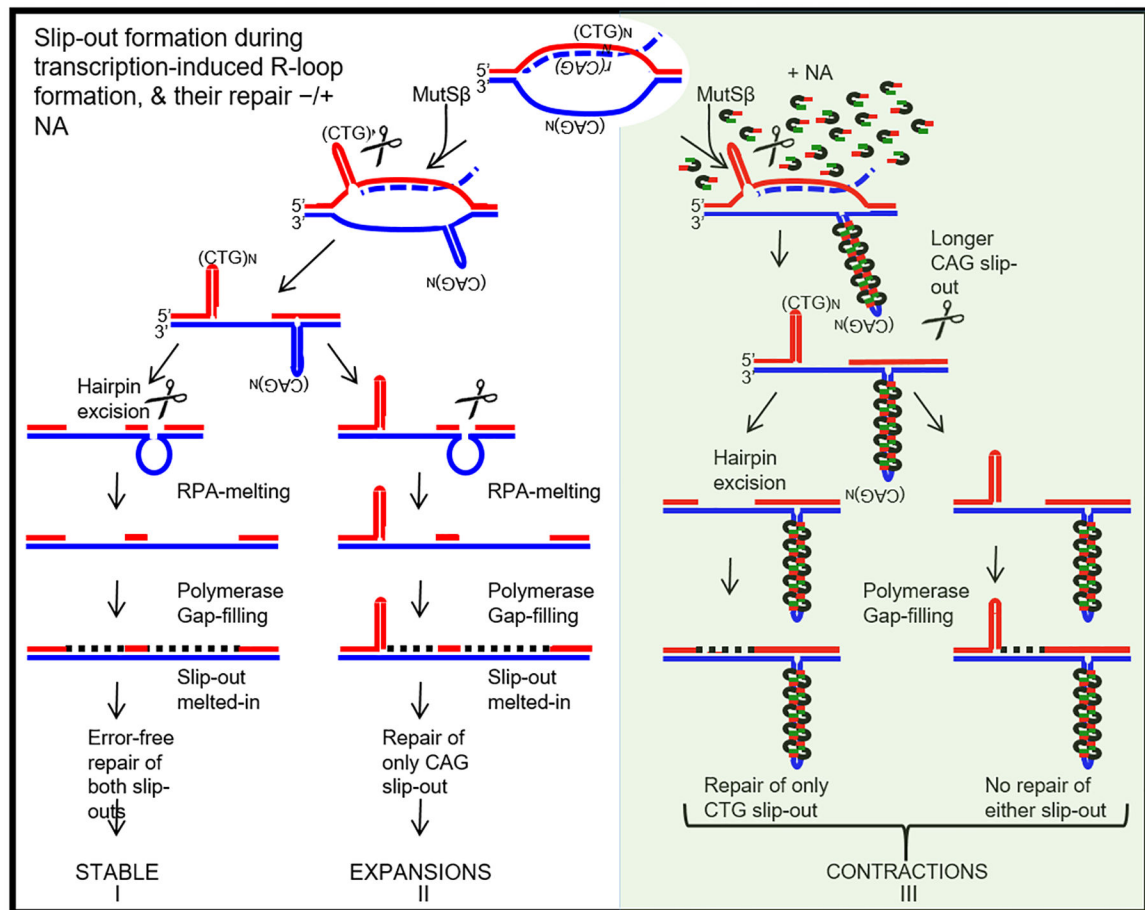


Figure 8 |. Schematic of the plausible mechanisms through which NA may induce contractions of expanded CAG tracts.

Schematic of transcription dependent slip-out formation and repair in the presence (green panel) or absence (white panel) of NA. See text for details.